Spin-orbit coupling from a two-component self-consistent approach. I. Generalized Hartree-Fock theory

Spin-Orbit Coupling from a Two-Component Self-Consistent Approach. Part I: Generalised Hartree-Fock Theory

Jacques K. Desmarais,[1, 2, 3, a)] Jean-Pierre Flament,[4] and Alessandro Erba[1, b)]
[1)] *Dipartimento di Chimica, Università di Torino, Via Giuria 5, 10125 Torino, Italy*
[2)] *Department of Geological Sciences, University of Saskatchewan, Saskatoon, SK S7N 5E2, Canada*
[3)] *Department of Physics and Engineering Physics, University of Saskatchewan, Saskatoon, SK S7N 5E2, Canada*
[4)] *Université de Lille, CNRS, UMR 8523 - PhLAM - Physique des Lasers Atomes et Molécules, 59000 Lille, France*

(Dated: 12 July 2019)

Formal and computational aspects are discussed of a self-consistent treatment of spin-orbit coupling within the two-component generalisation of the Hartree-Fock theory. A molecular implementation into the CRYSTAL program is illustrated, where the standard one-component code (typical of Hartree-Fock and Kohn-Sham spin-unrestricted methodologies) is extended to work in terms of two-component spinors. When passing from a one- to a two-component description, the Fock and density matrices become complex. Furthermore, apart from the $\alpha\alpha$ and $\beta\beta$ diagonal spin blocks, one has also to deal with the $\alpha\beta$ and $\beta\alpha$ off-diagonal spin blocks. These latter blocks require special care as, for open-shell electronic configurations, certain constraints of the one-component code have to be relaxed. This formalism intrinsically allows to treat local magnetic torque as well as non-collinear magnetization and orbital current-density. An original scheme to impose a specified non-collinear magnetization on each atomic center as a starting guess to the self-consistent procedure is presented. This approach turns out to be essential to surpass local minima in the rugged energy landscape and allow possible convergence to the ground-state solution in all of the discussed test cases.

Keywords: Spin-orbit coupling, exact exchange, CRYSTAL program, non-collinear magnetization, magnetic torque

I. INTRODUCTION

The most practical combination of quantum theory and the theory of relativity is governed by a system of four coupled complex equations and this system is colledtively called the Dirac equation.[1] There are two classes of relativistic effects which emerge from the Dirac equation and are not present in its non-relativistic counterpart (the Schrödinger equation). The first class is described by scalar operators and therefore comprises of what are called scalar-relativistic (SR) effects, such as mass-velocity and Darwin ones.[1–3] In the description of the electronic structure of a system, scalar effects manifest as relativistic corrections to the electron mass, and generally result in the direct stabilization (or contraction) of s- and p-type energy levels as well as indirect (through screening from more internal shells) destabilization of d-type energy levels.[2] The second class of relativistic effects is described by vector operators that are collectively referred to as spin-orbit (SO) or spin-orbit coupling (SOC) terms. The SOC refers to the coupling of the spin of an electron with its orbital motion. This coupling not only shifts the electronic levels of the system, but, in contrast to SR effects, also change the symmetry of the electronic states. This means that in heavy-element systems, where the SOC is strong, it can be necessary to include it in calculations even for a qualitatively correct description of the electronic structure. The SOC effect can be explained by the creation of a relativistic magnetic field induced by charged particles in motion relative to a reference electron. This magnetic field in turn couples with the field created by the spin of the reference electron.[3]

The most straightforward way to include SOC or SR effects in electronic structure calculations would be through a direct application of Dirac's complex-four-component equation as generalized to many-electron systems.[1–4] From a practical point of view, the corresponding equations are never solved exactly and Lorentz invariance is never achieved. Indeed, even when using the simple Hartree-Fock (HF) approximation on a many-electron atom within the full four-component scheme, no exact analytical form exists for the electron-electron operator (at variance with its non-relativistic counterpart), so that it must be approximated. This is typically done by including either the so-called Coulomb, Coulomb-Breit, or Coulomb-Gaunt terms.[1,3] Other times, the SOC is not included in the HF step, but only later, at the same stage as electronic correlation, in the so-called spin-orbit configuration-interaction (SO-CI) approaches.[5,6] For very heavy atoms, however, the splitting of the electronic levels caused by SOC can be of the same order or even greater than that caused by electronic correlation.[1–3,7] So it is clearly preferable to include SOC

[a)] Electronic mail: jkd788@mail.usask.ca
[b)] Electronic mail: alessandro.erba@unito.it

as early and as explicitly as possible in the calculation procedure.

It turns out that, in the description of the electronic states of a system (especially the valence states of chemical interest), two of the four components of Dirac's equation (the so-called large components) are more dominant. In many fields, it is therefore a common practice to approximate Dirac's equation by not explicitly treating the two less important (small) components. This is achieved by invoking proper decoupling transformations.[8,9] The resulting methodologies are known as two-component theories. These include the ZORA, FORA and IORA (zeroth-, first- and infinite-order regular-approximations),[10–13] Douglas-Kroll-Hess approach,[8] and the relatively more recent X2C (exact two-component) method.[14]

Yet another popular way to include relativistic effects in electronic structure calculations in a mixed two- and four-component approach, is through relativistic effective-core potentials (RECPs). These are effective potentials representing frozen configurations of core electrons that are fitted to comparatively very accurate single-atom relativistic four-component calculations.[15–18] These RECPs are then used to solve a two-component version of Dirac's equation for the many-body system. In general, this method might suffer from the frozen-core approximation. However, from a practical point of view, this approach may provide a better description than explicit four-component all-electron methods because the approximation of the electron-electron operator in the relativistic Hamiltonian can be pushed further at the single-atom stage during the RECP fitting in the core-region (where relativistic effects are more important) than in the study of the many-atom system.[19]

Nevertheless, unfortunately, in many programs for quantum-chemical calculations, the use of RECPs is limited to only treating SR effects, but not SOC. This is often the case purely for technical reasons. Indeed, the inclusion of only SR effects through RECPs poses no major challenges to the programmer, as the same structure of the existing code for calculations with non-relativistic ECPs can be maintained. This is no longer the case if SOC effects are to be also included in the calculation through the RECPs. In this case, the one-component real algebra scalar-relativistic or non-relativistic code (with non-relativistic point-symmetry exploitation) needs to be generalised to two-component eigenfunctions (spinors), complex algebra and relativistic space-spin symmetry (i.e. double-group symmetry). Significant efforts have been made in recent years in molecular codes along this direction to include SOC effects with RECPs in the self-consistent field (SCF) procedure of the NWChem code,[20,21] the Turbomole code,[22,23] and the Dirac code.[24,25] We stress that some of these codes already included SOC effects before these newer developments, through all-electron methodologies.

Here we discuss the generalisation of the Crystal code[26] to a two-component description of SOC through RECPs. The Crystal program uses a basis-set of Gaussian-type atom-centered functions to perform HF and density functional theory (DFT) calculations on finite molecular systems as well as on extended periodic systems in one, two or three dimensions. In the field of electronic structure calculations of periodic systems, the overwhelming majority of calculations are performed with the DFT, with the possible inclusion of a fraction of exact Fock exchange (as in hybrid functionals), and by using one-component codes that do not allow for SOC effects to be treated self-consistently. For example, the Vasp[27], Wien2k[28] and Fleur programs can treat SOC only in a non self-consistent way, as a post-SCF perturbation, after performing either a one- or two-component non- or scalar-relativistic SCF.[29,30] These non self-consistent methods are expected to be reliable only if the SOC is weak and the induced splitting of the energy levels small. In this respect, the most notable exception is represented by the Quantum-Espresso code,[31,32] where a self-consistent treatment of SOC from RECPs within the DFT has been implemented for solids.[33] The Amsterdam density functional (ADF) package also allows for self-consistent treatment of SOC in solids through the ZORA approach.[34] More recently, work has been done towards the treatment of SOC in solids with the GW theory.[35,36] A four-component periodic Kramers-Restricted Kohn-Sham implementation has been recently published.[37] We are not aware of any public implementation of self-consistent SOC-DFT for solids that takes into explicit account exact Fock exchange, despite it plays a crucial role in the description of a number of SOC-related physical effects (local magnetic torque, non-collinear magnetism, orbital current-density), as we are going to discuss in the present two-part paper.

As a first step towards the self-consistent treatment of SOC effects with an explicit account of exact Fock exchange, here we discuss formal and computational aspects of a molecular implementation based on the use of RECPs into the Crystal program. We discuss the self-consistent inclusion of SOC in the HF theory in Part I and the corresponding treatment within collinear and non-collinear DFT (in its local density, generalised-gradient and hybrid formulations) in Part II. In particular, in Part II we will address the accuracy, numerical robustness, and computational efficiency of the different flavors of non-collinear DFT reported in the literature and we will present a new formulation, which ensures higher numerical stability and efficiency.[38] The extension of the presented methodology to the description of extended periodic systems represents a near-future development and will be presented in forthcoming publications.

In Part I of the paper, we review all formal aspects of the most general variant of the two-component theory for the self-consistent inclusion of SOC in HF and Kohn-Sham (KS) calculations: the so-called Kramers-unrestricted (KU) approach. The KU theory is the most suitable for treating both open-shell and closed-shell elec-

tronic configurations within a single-determinantal description. The self-consistent treatment of SOC in open-shell electronic configurations is particularly challenging as it involves the breaking of certain symmetries that are usually exploited in one-component codes. In addition to Hermitian $\alpha\alpha$ and $\beta\beta$ spin blocks, also non-Hermitian $\alpha\beta$ and $\beta\alpha$ spin blocks of the Fock, or KS, and density matrices have to be considered. Granted, while the $\alpha\beta$ and $\beta\alpha$ are not individually Hermitian for open-shell systems, of course the total Fock, KS and density matrices are still Hermitian. The importance of the Fock exchange term in providing an indirect magnetic torque as well as a correct description of the orbital current-density, through its dependence on specific blocks of the density matrix, is discussed. This will become particularly crucial when different non-collinear formulations of the DFT will be illustrated in Part II.

Despite the formal difficulties in treating SOC for open-shell systems, it is also particularly rewarding, because these are exactly the same systems in which SOC is most important.[39–42] Indeed, the self-consistent treatment of SOC using approaches similar to the one described here allows for a proper description of systems containing heavy and magnetic elements as has been done for U by Wiegand *et al.*[19] and Zhang,[20] for Pb by Armbruster *et al.*,[22] for Au by Zeng *et al.*,[43] for Fe and Pt by Tsujikawata *et al.*,[44] or for Fe and Cu by Pacchioni *et al.*[45]

The inclusion of SOC often makes the electronic energy landscape very complicated, resulting in the presence of many local minima (metastable electronic states) and multiple global minima (i.e. degenerate ground state electronic configurations), even in very simple molecular systems, as will be shown in this paper. As for strongly correlated systems characterized by several electronic metastable states,[46] the starting guess for the electronic configuration (i.e. density matrix) of the system is of critical importance for the SCF procedure. In Part I of the paper, we present a strategy to modify a standard atomic guess for the density matrix so as to impose specified orientations for the electronic magnetization on each atomic center. We present some examples on small molecular systems where we show how calculations performed with different starting guesses often results in different final electronic states.

Finally, in Part I we document the correctness of the implementation, and we comment on its comparative numerical accuracy and efficiency against the existing similar public implementations.

II. FORMAL ASPECTS

In this section, we introduce some general concepts of relativistic quantum-chemistry and, in particular, we present formal aspects of the self-consistent treatment of spin-orbit coupling within a two-component generalisation of the Hartree-Fock theory. Regular font bold symbols (eg. $\mathbf{A}, \mathbf{a}$) are used for vector and matrix quantities in spin-space. Underlined font bold symbols (eg. $\underline{\mathbf{A}}, \underline{\mathbf{a}}$) are used for vector and matrix quantities in other spaces (for example Euclidean space). Hats are used for operators (eg. $\hat{A}, \hat{a}$) and if it is convenient to adopt a matrix representation of operators, these are also denoted by a bold-hat notation (eg. $\hat{\mathbf{A}}, \hat{\mathbf{a}}, \hat{\underline{\mathbf{A}}}, \hat{\underline{\mathbf{a}}}$). In this paper, all formulae are presented in atomic units and the bra-ket notation is reserved for eigenfunctions of spin operators, unless explicitly stated otherwise.

A. Spinors and Spin-Orbit Coupling Hamiltonians

The SOC is represented mathematically by a complex matrix operator, which acts on complex two-component vector quantities (spinors), which have the following representation in the spin basis:[1,2]

$$\boldsymbol{\Psi}_i = \langle \mathbf{s}|\boldsymbol{\psi}_i^{\alpha}\rangle + \langle \mathbf{s}|\boldsymbol{\psi}_i^{\beta}\rangle = \begin{pmatrix} \psi_i^{\alpha} \\ 0 \end{pmatrix} + \begin{pmatrix} 0 \\ \psi_i^{\beta} \end{pmatrix} . \tag{1}$$

In a one-electron atom, the SO operator has the following functional form:[4]

$$\hat{\mathbf{h}}_{\mathrm{SO}}(\underline{\mathbf{r}}) = \hat{\xi}(r)\hat{\underline{\mathbf{L}}}\cdot\hat{\underline{\mathbf{S}}} \, , \tag{2}$$

where $r = |\underline{\mathbf{r}}|$ is the magnitude of the position vector $\underline{\mathbf{r}}$, and $\hat{\underline{\mathbf{S}}}$ and $\hat{\underline{\mathbf{L}}}$ are the spin and angular-momentum operators. As a matter of fact, SO operators sharing a similar functional form, consisting of a product of radial, spin and angular-momentum operators (or a sum of such products) is also a common approximation for many practical calculations on molecules and periodic systems.[1,20,22,24,33] Such a mono-electronic operator is somewhat of a natural choice to describe spin-same-orbit (SSO) interactions (those between the spin and orbit of the same electron). On the other hand, spin-other-orbit (SOO) interactions (those between the spin and orbit of different electrons), would be more naturally represented using a bi-electronic operator.[1] In a two-component spinor basis, the spin operator $\hat{\underline{\mathbf{S}}}$ adopts the following representation:[1]

$$\hat{\underline{\mathbf{S}}} = \left(\hat{\mathbf{S}}_x, \hat{\mathbf{S}}_y, \hat{\mathbf{S}}_z\right)^{\mathrm{T}} \quad \text{with} \quad \hat{\mathbf{S}}_c = \frac{1}{2}\hat{\boldsymbol{\sigma}}_c \, , \tag{3}$$

where $c = x, y, z$ labels a Cartesian component and the Pauli matrices $\hat{\boldsymbol{\sigma}}_c$, are defined as follows:

$$\hat{\boldsymbol{\sigma}}_x = \begin{pmatrix} 0 & 1 \\ 1 & 0 \end{pmatrix} \quad \hat{\boldsymbol{\sigma}}_y = \begin{pmatrix} 0 & -i \\ i & 0 \end{pmatrix} \quad \hat{\boldsymbol{\sigma}}_z = \begin{pmatrix} 1 & 0 \\ 0 & -1 \end{pmatrix} . \tag{4}$$

The operators $\hat{\mathbf{S}}_x, \hat{\mathbf{S}}_y, \hat{\mathbf{S}}_z, \hat{\underline{\mathbf{S}}}$ have an associated spin-quantum number $s = 1/2$ and magnetic spin quantum number $m_s = \pm 1/2$, which determine their action on their associated eigenfunctions, including $|\boldsymbol{\alpha}\rangle$ and $|\boldsymbol{\beta}\rangle$, which are expressed as follows in the spin basis:

$$\langle \mathbf{s}|\boldsymbol{\alpha}\rangle = \begin{pmatrix} 1 \\ 0 \end{pmatrix} \quad \text{and} \quad \langle \mathbf{s}|\boldsymbol{\beta}\rangle = \begin{pmatrix} 0 \\ 1 \end{pmatrix} . \tag{5}$$

The angular-momentum operator $\underline{\hat{\mathbf{L}}}$, which instead only acts on the spatial part of the spinors, can be represented as follows in the position basis:

$$\underline{\hat{\mathbf{L}}} = \left(\hat{L}_x, \hat{L}_y, \hat{L}_z\right)^{\mathrm{T}} = -i\left(\underline{\hat{\mathbf{r}}} \times \underline{\hat{\boldsymbol{\nabla}}}\right) \ . \tag{6}$$

Similarly, the operators $\hat{L}_x, \hat{L}_y, \hat{L}_z, \underline{\hat{\mathbf{L}}}$ have an associated angular-momentum quantum number $l \in \{0, 1, 2, ...\}$ and magnetic quantum number $m \in \{-l, -(l-1), ..., 0, ..., (l-1), l\}$, which quantify their action on their respective eigenfunctions. For the atomic case, the presence of the SO operator implies that the Hamiltonian no-longer commutes with $\underline{\hat{\mathbf{S}}}$ and $\underline{\hat{\mathbf{L}}}$, so that the s, m_s, l, m are no-longer good quantum numbers, and hence cannot be used to label the spinors.[1] However, the quantum numbers s, m_s, l, m are still useful concepts, to label the functions on which the spinors are expanded. For example, in our implementation, we expand spinors in a set of atom-centered spin-orbitals $\boldsymbol{\chi}^{\sigma}$ ($\sigma = \alpha$ or β), which are eigenfunctions of $\underline{\hat{\mathbf{S}}}$ and $\underline{\hat{\mathbf{L}}}$, and can be expressed as follows in the spin-position basis:

$$\langle \underline{\mathbf{r}}, \mathbf{s} | \boldsymbol{\chi}^{\sigma} \rangle = R(r) Y_l^m(\underline{\mathbf{r}}) \langle \mathbf{s} | \boldsymbol{\sigma} \rangle \equiv \langle \underline{\mathbf{r}}, \mathbf{s} | \mathbf{l}, \mathbf{m} \rangle \ , \tag{7}$$

where $R(r)$ is a radial function (in our case a linear combination of Gaussian functions) and Y_l^m are real-solid spherical harmonics. It turns out that for atoms, it is still possible to define a new operator (the total angular-momentum) $\underline{\hat{\mathbf{J}}} = \underline{\hat{\mathbf{L}}} + \underline{\hat{\mathbf{S}}}$, which does commute with the Hamiltonian. In analogy to $\underline{\hat{\mathbf{L}}}$, $\underline{\hat{\mathbf{J}}}$ has associated quantum numbers $j = \left|l \pm 1/2\right|$, and $m_j \in \{-j, -(j-1), ..., 0, ..., (j-1), j\}$. These can also be useful to label the functions on which the spinors are expanded. Nonetheless, in the general polyatomic molecular case, the spinors are not eigenfunctions of any of $\underline{\hat{\mathbf{J}}}, \underline{\hat{\mathbf{L}}}, \underline{\hat{\mathbf{S}}}$. In this light, it is also useful to introduce the spin and angular-momentum ladder (or creation-annihilation) operators:

$$\hat{L}_{\pm} = \hat{L}_x \pm i\hat{L}_y \ ; \tag{8}$$

$$\hat{\mathbf{S}}_{\pm} = \hat{\mathbf{S}}_x \pm i\hat{\mathbf{S}}_y \ , \tag{9}$$

where the action of $\hat{\mathbf{S}}_{\pm}$ on the spin states $|\boldsymbol{\alpha}\rangle$, $|\boldsymbol{\beta}\rangle$ is:

$$\hat{\mathbf{S}}_+|\boldsymbol{\alpha}\rangle = |\mathbf{0}\rangle \quad \hat{\mathbf{S}}_+|\boldsymbol{\beta}\rangle = |\boldsymbol{\alpha}\rangle \ ; \tag{10}$$

$$\hat{\mathbf{S}}_-|\boldsymbol{\alpha}\rangle = |\boldsymbol{\beta}\rangle \quad \hat{\mathbf{S}}_-|\boldsymbol{\beta}\rangle = |\mathbf{0}\rangle \ , \tag{11}$$

and similarly, the action of the $\hat{L}_{\pm}$ (or $\hat{\mathbf{J}}_{\pm}$) on their eigenfunctions raises and lowers the quantum number m (or m_j).

In this paper we work with the following Hamiltonian that acts on two-component spinors:

$$\hat{\mathbf{H}} = \sum_k \left[\hat{h}_0(\underline{\mathbf{r}}_k)\hat{\boldsymbol{\sigma}}_0 + \hat{\mathbf{h}}_{\mathrm{SO}}(\underline{\mathbf{r}}_k)\right] + \hat{\mathbf{V}}_{ee} + \hat{V}_{NN} \ , \tag{12}$$

where $\hat{\boldsymbol{\sigma}}_0$ is the identity matrix in spin-space, k is an index that labels the electrons with coordinates $\underline{\mathbf{r}}_k$, $\hat{V}_{NN}$ is the nuclear-nuclear potential and $\hat{h}_0$ is a mono-electronic operator containing the SR, kinetic, and nuclear-electron interaction terms. We are going to show in Section II B below that the SOC operator in Eq. (12) has a somewhat similar functional form to the one presented in Eq. (2). Finally, $\hat{\mathbf{V}}_{ee}$ is the electron-electron interaction operator, which is at least in part bi-electronic. Since the Hamiltonian acts on two-component spinors, it has a 2×2 complex-matrix structure in spin-space, similarly to the $\hat{\boldsymbol{\sigma}}_c$ Pauli matrices introduced in Eq. (4). The four blocks of the matrix are denoted as the $\alpha\alpha, \alpha\beta, \beta\alpha$ and $\beta\beta$ spin-blocks:

$$\hat{\mathbf{H}} = \begin{pmatrix} \hat{\mathbf{H}}^{\alpha\alpha} & \hat{\mathbf{H}}^{\alpha\beta} \\ \hat{\mathbf{H}}^{\beta\alpha} & \hat{\mathbf{H}}^{\beta\beta} \end{pmatrix} \ . \tag{13}$$

This is in contrast to the non- or scalar-relativistic approach where operators have a 2×1 real structure in spin-space for open-shell systems (i.e. the $\alpha\alpha$ and $\beta\beta$ blocks) or 1×1 real structure for closed-shell systems.

B. Relativistic Effective Core Potentials for Spin-Orbit Coupling

In our approach, the SR and SO effects are both treated using the RECP method.[47] This method is nowadays routine in quantum-chemistry for treating SR effects, but has recently also gained popularity in the last decade for treating SOC in molecules,[20,22,24] and solids.[33] In this approach, core-core and core-valence electron interactions are represented using effective potentials, whose parameters are extracted from fitting to atomic four-component Dirac-Fock calculations. The parameters of the potentials are obtained using the energy-adjusted or shape-consistent methods.[48,49] Through this fitting procedure, the RECPs inherently take care of the SO and SR effects for core-core interactions. SR and SO effects (which are most important near the core) are therefore neglected for valence-valence interactions. In this way, all relativistic effects that are left to be treated variationally are the core-valence SO and SR interactions.

In our implementation, the core SR and SO operators are mono-electronic ones, act on two-component spinors, and adopt the form originally proposed by Ermler, Pitzer and co-workers.[47,50] In this approach, all relativistic (core-core SR and SO, core-valence SR and SO) and non-relativistic core-core and core-valence effects are represented using an effective-core potential operator $\hat{\mathbf{U}}^{\mathrm{REP}}$, which can be written as a sum of atom-centered operators $\hat{\mathbf{U}}_a^{\mathrm{REP}}$:

$$\hat{\mathbf{U}}^{\mathrm{REP}}(\underline{\mathbf{r}}) = \sum_a^N \hat{\mathbf{U}}_a^{\mathrm{REP}}(\underline{\mathbf{r}} - \underline{\mathbf{r}_\mathbf{a}}) \ , \tag{14}$$

where N is the number of atoms in the system and $\underline{\mathbf{r}_\mathbf{a}}$ are their positions. In fact, as we will show below, the $\hat{\mathbf{U}}^{\mathrm{REP}}$ can be subdivided into an average relativistic-effective

potential term $\hat{U}^{\mathrm{AREP}}$ representing all non- and scalar-relativistic effects, as well as a SO operator $\hat{\mathbf{h}}_{\mathrm{SO}}$:

$$\hat{\mathbf{U}}^{\mathrm{REP}}(\underline{\mathbf{r}}) = \hat{U}^{\mathrm{AREP}}(\underline{\mathbf{r}}) + \hat{\mathbf{h}}_{\mathrm{SO}}(\underline{\mathbf{r}}) \; . \tag{15}$$

Henceforth the sum over centers in Eq. (14) is made implicit. When using effective-core potentials as done here, the $\hat{\mathbf{h}}_{\mathrm{SO}}$ is sometimes referred to as the $\hat{\mathbf{U}}^{\mathrm{SOREP}}$ in the litterature. The effective-core potential operator is expanded as a product of radial and angular operators:[47]

$$\begin{aligned}\hat{\mathbf{U}}^{\mathrm{REP}}(\underline{\mathbf{r}}) &= \hat{U}^{\mathrm{REP}}_{LJ}(r) \\ &+ \sum_{l=0}^{L} \sum_{j=j_\beta}^{j_\alpha} \left[\hat{U}^{\mathrm{REP}}_{lj}(r) - \hat{U}^{\mathrm{REP}}_{LJ}(r)\right] \hat{\mathbf{P}}_{l,j}(\theta,\phi)\end{aligned} \tag{16}$$

In the above, L is the largest angular-momentum quantum number used to describe the core (usually chosen as equal-to or one higher than in the valence basis-set), J is the corresponding total-angular momentum ($J = \left|L \pm 1/2\right|$), and we have used the notation $j_\alpha = \left|l + 1/2\right|$ and $j_\beta = \left|l - 1/2\right|$. The $\hat{U}^{\mathrm{REP}}_{lj}(r)$ are radial potentials fitted to a linear combination of solid-Gaussian functions.[51] Given that the $\hat{U}^{\mathrm{REP}}_{lj}(r)$ are dependent on the total- and angular-momentum l and j, projection operators are necessary to ensure that each radial operator acts on functions of the appropriate l and j species. The θ and ϕ are the inclination and azimuthal polar angles of the electron coordinates. In our case, the angular projectors are defined as:

$$\hat{\mathbf{P}}_{l,j}(\theta,\phi) = \sum_{m_j=-j}^{j} |\mathbf{l},\mathbf{j},\mathbf{m_j}\rangle\langle\mathbf{l},\mathbf{j},\mathbf{m_j}| \; . \tag{17}$$

The $\hat{\mathbf{P}}_{l,j}$ are generally complex operators acting on both the spatial and spin part of the spinors. More specifically, the $|\mathbf{l},\mathbf{j},\mathbf{m_j}\rangle$ are chosen as two-component, complex eigenfunctions of the Pauli Hamiltonian,[47] which is an approximation to the Dirac Hamiltonian.

The average-relativistic effective potential $\hat{U}^{\mathrm{AREP}}$ reads:[47,50]

$$\begin{aligned}\hat{U}^{\mathrm{AREP}}(\underline{\mathbf{r}}) &= \hat{U}^{\mathrm{AREP}}_{L}(r) \\ &+ \sum_{l=0}^{L} \left[\hat{U}^{\mathrm{AREP}}_{l}(r) - \hat{U}^{\mathrm{AREP}}_{L}(r)\right] \hat{P}_l(\theta,\phi) \; ,\end{aligned} \tag{18}$$

where, the angular projectors $\hat{P}_l$ are defined as:

$$\hat{P}_l(\theta,\phi) = \sum_{m=-l}^{l} |l,m\rangle\langle l,m| \; . \tag{19}$$

In contrast to $\hat{\mathbf{P}}_{l,j}$, the operators $\hat{P}_l$ now only act on the spatial part of the spinors. They are defined using the $|l,m\rangle$, which are one-component, real eigenfunctions of the SR Dirac Hamiltonian.[47] The $\hat{U}^{\mathrm{AREP}}_{l}(r)$ in turn are averaged, purely scalar-relativistic radial potentials, defined in terms of quantities in Eq. (16) as:[47,50]

$$\hat{U}^{\mathrm{AREP}}_{l}(r) = \frac{1}{2l+1}\left[l\hat{U}^{\mathrm{REP}}_{l,j_\beta}(r) + (l+1)\hat{U}^{\mathrm{REP}}_{l,j_\alpha}(r)\right] \; . \tag{20}$$

The SO part of the operator can then be defined as the difference between the fully-relativistic $\hat{\mathbf{U}}^{\mathrm{REP}}$ and the SR $\hat{U}^{\mathrm{AREP}}$ and takes the form:[52]

$$\hat{\mathbf{h}}_{\mathrm{SO}}(\underline{\mathbf{r}}) = \frac{1}{2}\sum_{l=1}^{L-1} \hat{\xi}_l(r) \left\{ l\hat{\mathbf{P}}_{l,j_\alpha}(\theta,\phi) - (l+1)\,\hat{\mathbf{P}}_{l,j_\beta}(\theta,\phi)\right\} \; , \tag{21}$$

where:

$$\hat{\xi}_l(r) = \frac{2}{2l+1}\left[\hat{U}^{\mathrm{REP}}_{l,j_\alpha}(r) - \hat{U}^{\mathrm{REP}}_{l,j_\beta}(r)\right] \; . \tag{22}$$

We note that the convention for expressing $\hat{\xi}_l(r)$ varies according to the authors up to an l-dependent factor, as can be seen, for instance by comparing Eq. (22), with those from Ref. 50 and 47. The advantage of the formulation above is that the $\hat{\mathbf{U}}^{\mathrm{REP}}$ is separated in the SR real term $\hat{U}^{\mathrm{AREP}}$ and the complex SO term $\hat{\mathbf{h}}_{\mathrm{SO}}$. As such, existing algorithms to evaluate SR effects from RECPs can be adapted to evaluate the $\hat{U}^{\mathrm{AREP}}$ integrals and new algorithms are only needed to evaluate the $\hat{\mathbf{h}}_{\mathrm{SO}}$ integrals. In our implementation, the $\hat{U}^{\mathrm{AREP}}$ integrals are evaluated by modification of existing routines in the CRYSTAL code,[26] based on a method proposed by McMurchie and Davidson[51] in a basis set of Cartesian Gaussian-type functions (CGTF). This approach is partly analytical (for angular and radial integrals of type I) and partly involves numerical quadrature (for radial integrals of type II).[51] The exact definition of the radial integrals of type I and II can be found in Ref. 51. The integrals over the $\hat{\mathbf{h}}_{\mathrm{SO}}$ are instead evaluated by modification of the routines of the ARGOS integral package,[53] again over CGTF using a closely-related approach to that proposed by McMurchie and Davidson. These CGTF integrals are subsequently transformed to a basis of spherical-Gaussian type functions up to angular momentum $l = 4$.[54]

Finally, we note that the mono-electronic form of the SO operator above in Eq. (21) reduces to:[1]

$$\hat{\mathbf{h}}_{\mathrm{SO}}(\underline{\mathbf{r}}) = \sum_{l=1}^{L-1} \hat{\xi}_l(r)\hat{P}_l(\theta,\phi)\hat{\underline{\mathbf{L}}}\cdot\underline{\hat{\mathbf{S}}}\hat{P}_l(\theta,\phi) \; , \tag{23}$$

which has a similar functional form to Eq. (2). As mentioned in Section II A, a mono-electronic operator is a natural choice for describing SSO interactions, but is not so natural for describing SOO interactions. However, in our case, SOO interactions are also implicitly included in the $\hat{\mathbf{h}}_{\mathrm{SO}}$ through the fitting procedure of the RECPs from four-component Dirac-Fock calculations.

C. Generalised Hartree-Fock Theory

We now discuss into some detail the present Hartree-Fock treatment including SOC interactions. Our implementation is based on a linear-combination of atomic-orbitals (LCAO) framework. As was anticipated in Section II A, the presence of the complex SOC operator implies that the molecular orbitals (MOs) are expressed in terms of the complex two-component spinors introduced in Eq. (1). The spinors, in turn are expanded in a set of n_f atomic spin-orbitals defined in Eq. (7):

$$\mathbf{\Psi}_i(\underline{\mathbf{r}}) = \sum_{\mu=1}^{n_f} c^{\alpha}_{\mu,i} \begin{pmatrix} \chi_\mu(\underline{\mathbf{r}}) \\ 0 \end{pmatrix} + c^{\beta}_{\mu,i} \begin{pmatrix} 0 \\ \chi_\mu(\underline{\mathbf{r}}) \end{pmatrix} , \tag{24}$$

where the $c^{\sigma}_{\mu,i}$ are the (generally) complex MO coefficients. Variation of the orbital coefficients, under the constraint of orthonormalization, to minimize the energy of the respective Slater determinant leads to Hartree-Fock-Roothaan-type equations which resemble closely the scalar- or non-relativistic procedure. More specifally, in our case the $c^{\sigma}_{\mu,i}$ satisfy the complex generalized HF (GHF) equations:[55]

$$\mathbf{Fc} = \mathbf{Sc}\boldsymbol{\epsilon} , \tag{25}$$

where the $\mathbf{S}$, $\mathbf{c}$, $\boldsymbol{\epsilon}$ are the usual overlap matrices and one-particle Fock eigenvector and diagonal-eigenvalue matrices, respectively, which have a size of $2n_f \times 2n_f$. The Fock (or Hamiltonian) matrix $\mathbf{F}$, is the matrix representation of the Hamiltonian introduced in Eq. (12) in the basis of atomic spin-orbitals. We can write Eq. (25) in a more explicit way to display its structure in spin-space as follows:

$$\begin{pmatrix} \mathbf{F}^{\alpha\alpha} & \mathbf{F}^{\alpha\beta} \\ \mathbf{F}^{\beta\alpha} & \mathbf{F}^{\beta\beta} \end{pmatrix} \begin{pmatrix} \mathbf{c}^{\alpha} \\ \mathbf{c}^{\beta} \end{pmatrix} = \begin{pmatrix} \mathbf{S}^{\alpha\alpha} & \mathbf{0}^{\alpha\beta} \\ \mathbf{0}^{\beta\alpha} & \mathbf{S}^{\beta\beta} \end{pmatrix} \begin{pmatrix} \mathbf{c}^{\alpha} \\ \mathbf{c}^{\beta} \end{pmatrix} \boldsymbol{\epsilon} . \tag{26}$$

The off-diagonal spin-blocks of $\mathbf{S}$ are nullified by mono-electronic spin-sum rules, as evidenced by Eq. (24). The $\mathbf{0}^{\sigma\sigma'}$ is a matrix of zeros. As in the above, when matrices do not have a double spin-index superscript, it is assumed that they have a size of $2n_f \times 2n_f$, unless explicitly stated otherwise. Matrices that do have a double spin-index superscript have a size of $n_f \times n_f$. The Fock matrix $\mathbf{F}$ is written as the sum of mono-electronic $\mathbf{h}$, as well as Coulomb $\mathbf{C}$ and exchange $\mathbf{K}$ contributions:

$$\mathbf{F} \equiv \mathbf{h} + \mathbf{C} + \mathbf{K} . \tag{27}$$

1. Mono-Electronic Integrals

The spin structure of the mono-electronic term $\mathbf{h}$ is as follows:

$$\begin{pmatrix} \mathbf{h}^{\alpha\alpha} & \mathbf{h}^{\alpha\beta} \\ \mathbf{h}^{\beta\alpha} & \mathbf{h}^{\beta\beta} \end{pmatrix} = \begin{pmatrix} \mathbf{h}_0^{\alpha\alpha} & \mathbf{0}^{\alpha\beta} \\ \mathbf{0}^{\beta\alpha} & \mathbf{h}_0^{\beta\beta} \end{pmatrix} + \begin{pmatrix} \mathbf{h}_{\mathrm{SO}}^{\alpha\alpha} & \mathbf{h}_{\mathrm{SO}}^{\alpha\beta} \\ \mathbf{h}_{\mathrm{SO}}^{\beta\alpha} & \mathbf{h}_{\mathrm{SO}}^{\beta\beta} \end{pmatrix} . \tag{28}$$

In the above, the $\hat{h}_0$ operator is the SR mono-electronic part, containing the AREP, valence kinetic, and valence-nuclear electrostatic terms. The matrix elements of the $\hat{h}_0$ operator are real and have the following symmetries:

$$[h_0^{\alpha\alpha}]_{\mu\nu} = [h_0^{\alpha\alpha}]_{\nu\mu} = \left[h_0^{\beta\beta}\right]_{\nu\mu} = \left[h_0^{\beta\beta}\right]_{\mu\nu} , \tag{29}$$

where the matrix elements are defined as:

$$\left[h_0^{\sigma\sigma'}\right]_{\mu\nu} = \langle \boldsymbol{\chi}_\mu^{\sigma} | \hat{h}_0 | \boldsymbol{\chi}_\nu^{\sigma'} \rangle . \tag{30}$$

From Eq. (23), and taking into account the form of the Pauli matrices from Eqs. (3) and (4), the matrix elements of the SO operator for the diagonal spin-blocks are:

$$\begin{aligned} [h_{\mathrm{SO}}^{\alpha\alpha}]_{\mu\nu} &= \sum_{l=1}^{L-1} \langle \boldsymbol{\chi}_\mu^{\alpha} | \hat{\xi}_l \hat{P}_l \hat{L}_z \hat{\mathbf{S}}_z \hat{P}_l | \boldsymbol{\chi}_\nu^{\alpha} \rangle \\ &= \frac{1}{2} \sum_{l=1}^{L-1} \langle \chi_\mu | \hat{\xi}_l \hat{P}_l \hat{L}_z \hat{P}_l | \chi_\nu \rangle . \end{aligned} \tag{31}$$

For the off-diagonal spin-blocks, using now also the spin and angular momentum ladder operators $\hat{L}_\pm$, $\hat{\mathbf{S}}_\pm$ defined in Eqs. (8) and (9):

$$\begin{aligned} \left[h_{\mathrm{SO}}^{\alpha\beta}\right]_{\mu\nu} &= \frac{1}{2} \sum_{l=1}^{L-1} \langle \boldsymbol{\chi}_\mu^{\alpha} | \hat{\xi}_l \hat{P}_l \hat{L}_- \hat{\boldsymbol{S}}_+ \hat{P}_l | \boldsymbol{\chi}_\nu^{\beta} \rangle \\ &= \frac{1}{2} \sum_{l=1}^{L-1} \langle \chi_\mu | \hat{\xi}_l \hat{P}_l \hat{L}_- \hat{P}_l | \chi_\nu \rangle . \end{aligned} \tag{32}$$

The SO matrix elements have the following symmetries, from the properties of the spin and angular momentum operators discussed in Eqs. (3) to (11), for the diagonal spin-blocks:

$$[h_{\mathrm{SO}}^{\alpha\alpha}]_{\mu\nu} = -\,[h_{\mathrm{SO}}^{\alpha\alpha}]_{\nu\mu} = \left[h_{\mathrm{SO}}^{\beta\beta}\right]_{\nu\mu} = -\left[h_{\mathrm{SO}}^{\beta\beta}\right]_{\mu\nu} , \tag{33}$$

and for the off-diagonal spin-blocks:

$$\left[h_{\mathrm{SO}}^{\alpha\beta}\right]_{\mu\nu} = -\left[h_{\mathrm{SO}}^{\alpha\beta}\right]_{\nu\mu} = \left[h_{\mathrm{SO}}^{\beta\alpha}\right]^*_{\nu\mu} = -\left[h_{\mathrm{SO}}^{\beta\alpha}\right]^*_{\mu\nu} . \tag{34}$$

In the above, the operator $\hat{L}_z$ is purely imaginary and the $\hat{L}_-$ is complex. As a consequence, the matrix elements of the $\alpha\alpha$ and $\beta\beta$ blocks of $\hat{\mathbf{h}}_{\mathrm{SO}}$ are purely imaginary, while those of the $\alpha\beta$ and $\beta\alpha$ blocks are complex. The symmetry properties of the matrix elements can be exploited in their construction, such that only one of the upper- or lower-triangular blocks of $\alpha\alpha$ and $\alpha\beta$ need to be explicitly calculated.

2. Bi-Electronic Integrals

To write a succinct expression for the real Coulomb $\mathbf{C}$ and complex exchange $\mathbf{K}$ matrix elements, we introduce the one-particle density matrix $\mathbf{D}$:

$$\left[D^{\sigma\sigma'}\right]_{\mu\nu} \equiv \sum_{i}^{occ} \left[c_{\mu i}^{\sigma}\right]^* c_{\nu i}^{\sigma'} , \tag{35}$$

where the index i runs over the occupied MOs and the density matrix is complex-Hermitian:

$$\left[D^{\sigma\sigma'}\right]_{\mu\nu} = \left[D^{\sigma'\sigma}\right]^*_{\nu\mu} \ . \tag{36}$$

The Coulomb and exchange matrix elements are written in terms of bi-electronic integrals:

$$\left(\boldsymbol{\chi}_\mu^\sigma \boldsymbol{\chi}_\nu^{\sigma'} | \boldsymbol{\chi}_\rho^{\sigma''} \boldsymbol{\chi}_\gamma^{\sigma'''}\right) \equiv (\chi_\mu\chi_\nu|\chi_\rho\chi_\gamma)\delta_{\sigma,\sigma'}\ \delta_{\sigma'',\sigma'''} \ , \tag{37}$$

with:

$$(\chi_\mu\chi_\nu|\chi_\rho\chi_\gamma) \equiv \iint d\underline{\mathbf{r}}_\mathbf{1} d\underline{\mathbf{r}}_\mathbf{2} \chi_\mu(\underline{\mathbf{r}}_\mathbf{1})\chi_\nu(\underline{\mathbf{r}}_\mathbf{1})\frac{1}{r_{12}}\chi_\rho(\underline{\mathbf{r}}_\mathbf{2})\chi_\gamma(\underline{\mathbf{r}}_\mathbf{2}) \ , \tag{38}$$

where $r_{12} = |\underline{\mathbf{r}}_\mathbf{1} - \underline{\mathbf{r}}_\mathbf{2}|$ and the Kronecker-delta functions appear from the matrix products in spin space. In this way, the Coulomb term may be written as:

$$\left[C^{\alpha\alpha}\right]_{\mu\nu} = \sum_{\rho,\gamma} (\chi_\mu\chi_\nu|\chi_\rho\chi_\gamma)\ \Re\left(\left[D^{\alpha\alpha}\right]_{\rho\gamma} + \left[D^{\beta\beta}\right]_{\rho\gamma}\right) \ , \tag{39}$$

where the $\Re$ is used to denote the real part of the argument (similarly, in the following the $\Im$ will be used for the imaginary part). The real Coulomb matrix elements have the following symmetries, for the diagonal spin-blocks

$$\left[C^{\alpha\alpha}\right]_{\mu\nu} = \left[C^{\alpha\alpha}\right]_{\nu\mu} = \left[C^{\beta\beta}\right]_{\nu\mu} = \left[C^{\beta\beta}\right]_{\mu\nu} \ , \tag{40}$$

while the off-diagonal spin-blocks are null, so that the overall structure in spin-space reads:

$$\mathbf{C} = \begin{pmatrix} \mathbf{C}^{\alpha\alpha} & \mathbf{0}^{\alpha\beta} \\ \mathbf{0}^{\beta\alpha} & \mathbf{C}^{\beta\beta} \end{pmatrix} \ . \tag{41}$$

The exchange terms are calculated as follows for both diagonal and off-diagonal spin-blocks:

$$\left[K^{\sigma\sigma'}\right]_{\mu\nu} = -\sum_{\rho,\gamma} (\chi_\mu\chi_\gamma|\chi_\nu\chi_\rho)\left[D^{\sigma'\sigma}\right]_{\rho\gamma} \ , \tag{42}$$

and the matrix elements are complex-Hermitian:

$$\left[K^{\sigma\sigma'}\right]_{\mu\nu} = \left[K^{\sigma'\sigma}\right]^*_{\nu\mu} \ . \tag{43}$$

As can be seen above, the exchange operator is the only one that generates terms for which elements of the $\alpha\alpha$ blocks cannot be related to those in the $\beta\beta$ blocks, and for which the lower triangular elements of the off-diagonal spin-blocks cannot be related to corresponding upper-triangular elements. This is a consequence of the lack of correspondence between $\alpha\alpha$ and $\beta\beta$ elements of the density matrix, as well as the non-Hermiticity of its off-diagonal spin-blocks in open-shell systems. Even though the off-diagonal spin-blocks of the density matrix are not individually Hermitian, of course the whole matrix is Hermitian. It is worth mentioning that since the Coulomb terms contain only the real part of the density matrix, their calculation is identical to the scalar- and non-relativistic approaches. This means that no modification of the existing SR code was necessary for calculating the Coulomb term. For the exchange term, the integrals are the same as in the SR code, but they now need to be combined with new blocks of the density matrix. In the calculation of the bi-electronic exchange integrals like those denoted in Eq. (42), the following permutation symmetries are exploited:

$$\chi_\mu \leftrightarrow \chi_\gamma, \quad \chi_\nu \leftrightarrow \chi_\rho \quad \text{and} \quad (\chi_\mu\chi_\gamma) \leftrightarrow (\chi_\nu\chi_\rho) \ , \tag{44}$$

so that the same integral can be used eight times for the construction of the Coulomb and exchange matrices. One difference with respect to the SR code is that when applying these permutations, the sign of the corresponding density matrix block must be reversed, see Eq. (36). Additionally, for open-shell systems, the off-diagonal spin-blocks are not necessarily Hermitian. This is in contrast to the SR code, in which the off-diagonal blocks are null, so that additional care must now be taken to associate the appropriate density-matrix block once the permutation is performed.

3. Energy

The total energy E is calculated using the trace operator Tr as follows:

$$E = \frac{1}{2}\left\{\mathrm{Tr}\left(\mathbf{h}\mathbf{D}^\dagger\right) + \mathrm{Tr}\left(\mathbf{F}\mathbf{D}^\dagger\right)\right\} \ . \tag{45}$$

Using the properties of the trace operator, as well as the Hermiticity of $\mathbf{h}, \mathbf{D}$ and $\mathbf{F}$, the energy can be partitioned into different contributions:

$$\begin{aligned} E = \Bigg\{ & \Re\left[\mathrm{Tr}\left(\mathbf{h}_0\mathbf{D}^\dagger\right)\right] + \Re\left[\mathrm{Tr}\left(\mathbf{h}_{\mathrm{SO}}\mathbf{D}^\dagger\right)\right] \\ & + \frac{1}{2}\Re\left[\mathrm{Tr}\left(\mathbf{C}\mathbf{D}^\dagger\right)\right] + \frac{1}{2}\Re\left[\mathrm{Tr}\left(\mathbf{K}\mathbf{D}^\dagger\right)\right]\Bigg\} \ . \end{aligned} \tag{46}$$

Working expressions for the traces above can be found in the Appendix.

4. Electron Density and Magnetization

The total (or particle-number) electron density can be calculated from the occupied two-component spinors as a product in the spin basis:

$$n(\underline{\mathbf{r}}) \equiv \sum_i^{occ} \boldsymbol{\Psi}_i^\dagger(\underline{\mathbf{r}})\boldsymbol{\Psi}_i(\underline{\mathbf{r}}) \ . \tag{47}$$

Developing this product using the Hermiticity of the density matrix of Eq. (36) yields:

$$n(\underline{\mathbf{r}}) = n^\Re_{\alpha\alpha}(\underline{\mathbf{r}}) + n^\Re_{\beta\beta}(\underline{\mathbf{r}}) \ , \tag{48}$$

where we now introduce the compact notation:

$$n^{\Re}_{\sigma\sigma'}(\underline{\mathbf{r}}) = \sum_{\mu\nu} \Re\Big[D^{\sigma\sigma'}\Big]_{\mu\nu} \chi_\mu(\underline{\mathbf{r}})\chi_\nu(\underline{\mathbf{r}}) \; ;$$
$$n^{\Im}_{\sigma\sigma'}(\underline{\mathbf{r}}) = \sum_{\mu\nu} \Im\Big[D^{\sigma\sigma'}\Big]_{\mu\nu} \chi_\mu(\underline{\mathbf{r}})\chi_\nu(\underline{\mathbf{r}}) \; . \quad (49)$$

Information on the spin-polarisation of the system is given by the magnetization vector $\underline{\mathbf{m}} = \big[m_x, m_y, m_z\big]$. Its Cartesian components are:[56]

$$m_c(\underline{\mathbf{r}}) \equiv \sum_i^{occ} \mathbf{\Psi}_i^\dagger(\underline{\mathbf{r}})\hat{\boldsymbol{\sigma}}_c\mathbf{\Psi}_i(\underline{\mathbf{r}}) \; . \quad (50)$$

Using the expression for the Pauli matrices in Eq. (4), as well as the Hermiticity of the density matrix, explicit expressions are obtained for each component:

$$m_x(\underline{\mathbf{r}}) = n^{\Re}_{\alpha\beta}(\underline{\mathbf{r}}) + n^{\Re}_{\beta\alpha}(\underline{\mathbf{r}}) \; ; \quad (51)$$
$$m_y(\underline{\mathbf{r}}) = n^{\Im}_{\alpha\beta}(\underline{\mathbf{r}}) - n^{\Im}_{\beta\alpha}(\underline{\mathbf{r}}) \; ; \quad (52)$$
$$m_z(\underline{\mathbf{r}}) = n^{\Re}_{\alpha\alpha}(\underline{\mathbf{r}}) - n^{\Re}_{\beta\beta}(\underline{\mathbf{r}}) \; . \quad (53)$$

We define the concept of collinear magnetization as a spatial distribution of $\underline{\mathbf{m}}$ which is everywhere parallel or anti-parallel. On the other hand, a non-collinear magnetization is a spatial distribution of the $\underline{\mathbf{m}}$ in which at least one point in space is associated with a value of $\underline{\mathbf{m}}$ that is not parallel or anti-parallel to that of the other points in space.[57] From Eq. (49), as well as Eqs. (51) and (52), the m_x and m_y are proportional to the real and imaginary parts of the off-diagonal spin-blocks of the density matrix, respectively. From Eq. (53), the m_z is proportional to the real part of the diagonal spin-blocks of the density matrix. In addition, from Eqs. (A.1), (A.2) and (A.4), for the calculation of the energy, we note that the SOC operator is the only one which combines integrals with the spin blocks of the density matrix that enter into the magnetization. The physical consequence of this is that the SOC operator is the only term which directly imparts an energy dependence on the orientation of the magnetization (sometimes called magnetic torque).[58] This is because the electron-spin couples with the geometry of the system (hence the orientation of the magnetization) through coupling with its orbital motion. Albeit, for some systems the exchange operator can also impart an indirect energy dependence on the orientation of the magnetization through the dependence of the operator on the density matrix in Eq. (42). The energy contribution from the exchange operator is also invariant to a global rotation of the spin-reference frame, while the SO contribution is sensitive to such rotations.

5. Non-Collinear Guess for the Density Matrix

Since the SOC operator is the only term in the Hamiltonian which imparts a direct energy dependence on the orientation of the magnetization, if the SOC is not very strong, the energy dependence will be very weak. So it is not guaranteed that the SCF procedure will always yield the optimal magnetization distribution. The starting guess for the magnetization distribution can therefore be important to ensure convergence to the lowest energy solution and for calculating properties which depend strongly on the direction of the magnetization.[59] In this light, we show here how a non-relativistic atomic starting guess for the density matrix (here referred to as $\mathbf{D}_{\rm col}$) - in our case calculated from an approach originally described by Clementi in Ref. 60 - can be generalized to impose a specified non-collinear magnetization on the individual atoms, as a starting point. Actually, the approach presented below would also work for other types of non-relativistic or scalar-relativistic atomic starting guess density matrices. To our knowledge, such an approach has not been presented before in the literature and yet represents an important tool for describing the electronic structure from a two-component SCF procedure, as will be explicitly shown in Section IV. In that section, we will show that for all of the tested cases the global minimum of the total energy can only be found through such modification of the guess.

Such an atomic guess density matrix is block-diagonal with each individual block spanning the AOs of each atom in the system. Given that the guess density matrix is Hermitian, in our implementation the manipulation of this matrix is done only on its upper triangular portion. Once the density matrix has been manipulated to impose the desired magnetization, it can then be Hermitised. Since the standard guess density matrix $\mathbf{D}_{\rm col}$ is non- or scalar-relativistic, for each individual atomic block, let us work in terms of its spin-polarization-dependent component:

$$\mathbf{D}^{\rm spin}_{\rm col}(a) = \Re\mathbf{D}^{\alpha\alpha}_{\rm col}(a) - \Re\mathbf{D}^{\beta\beta}_{\rm col}(a) \; , \quad (54)$$

and spin-polarization-independent component:

$$\mathbf{D}^{\rm tot}_{\rm col}(a) = \Re\mathbf{D}^{\alpha\alpha}_{\rm col}(a) + \Re\mathbf{D}^{\beta\beta}_{\rm col}(a) \; , \quad (55)$$

where a is again an index that labels the atoms in the system. The subscript "col" indicates that the above matrices are related to collinear magnetization distributions, because of the non- or scalar-relativistic nature of the atomic calculation. These matrices are purely real and the only spin-blocks which are potentially non-zero are the $\alpha\alpha$ and $\beta\beta$ ones. In what follows, we propose to combine and scale these real $\alpha\alpha$ and $\beta\beta$ blocks to define a new guess, which will be instead complex and also to set the elements of the off-diagonal $\alpha\beta$ and $\beta\alpha$ blocks to non-zero values, so as to impose a desired non-collinear magnetization by exploiting the relation between the density matrix and the magnetization, from Eq. (50).

In the standard procedure, given that the atomic guess is scalar- or non-relativistic, then the $\mathbf{D}^{\rm spin}_{\rm col}(a)$ could be used to impose an associated collinear magnetization $\underline{\mathbf{m}}^{\rm col}(a) = (0, 0, m^{\rm col}_z(a))$, with magnitude $m^{\rm col}(a) = \big|\underline{\mathbf{m}}^{\rm col}(a)\big| \equiv m^{\rm col}_z(a)$. In order to instead impose a non-

collinear magnetization $\underline{\mathbf{m}}(a)$, we define polar θ_a and azimuthal ϕ_a angles, which will be used to locally re-define the orientation of the magnetization on each atomic center, without changing its magnitude. The angles θ_a, and ϕ_a can be interpreted pictorially with the help of the diagram in Figure 1. Since the relevant density matrices are atomic, we are free to choose different variables θ_a and ϕ_a on different atoms. In this way, we define the atomic non-collinear magnetization as follows:

$$\begin{aligned} \underline{\mathbf{m}}(a) &= m^{\rm col}(a)\underline{\mathbf{w}}(a) \\ \underline{\mathbf{w}}(a) &= \big(\sin(\theta_a)\sin(\phi_a), \sin(\theta_a)\cos(\phi_a), \cos(\theta_a)\big) \end{aligned} \quad , (56)$$

where $\underline{\mathbf{w}}(a)$ is a unitary vector, defined locally on each center, which orients the magnetization according to the polar angles θ_a and ϕ_a (see Figure 1). Therefore the relative magnitude of the Cartesian components of $\underline{\mathbf{m}}(a)$ is determined solely from the components of $\underline{\mathbf{w}}(a)$. From Eq. (50), the Cartesian components of $\underline{\mathbf{m}}(a)$ are proportional to distinct spin-blocks of the density matrix, as explicitly shown below. A non-collinear guess for the density matrix $\mathbf{D}$ can be obtained by distributing the collinear magnetization of the standard guess $\mathbf{D}_{\rm col}$ - in proportions determined by the Cartesian components of $\underline{\mathbf{w}}(a)$ - over its different spin-blocks so as to ensure the desired non-collinear magnetization according to Eqs. (51) - (53):

$$\begin{aligned} \Re\mathbf{D}^{\alpha\beta}(a) &= \Re\mathbf{D}^{\beta\alpha}(a) = \frac{1}{2}\sin(\theta_a)\sin(\phi_a)\mathbf{D}^{\rm spin}_{\rm col}(a) \; ; \\ \Im\mathbf{D}^{\alpha\beta}(a) &= -\Im\mathbf{D}^{\beta\alpha}(a) = \frac{1}{2}\sin(\theta_a)\cos(\phi_a)\mathbf{D}^{\rm spin}_{\rm col}(a) \; ; \\ \Re\mathbf{D}^{\alpha\alpha}(a) &= \frac{1}{2}\left[\mathbf{D}^{\rm tot}_{\rm col}(a) + \cos(\theta_a)\mathbf{D}^{\rm spin}_{\rm col}(a)\right] \; ; \\ \Re\mathbf{D}^{\beta\beta}(a) &= \frac{1}{2}\left[\mathbf{D}^{\rm tot}_{\rm col}(a) - \cos(\theta_a)\mathbf{D}^{\rm spin}_{\rm col}(a)\right] \; ; \\ \Im\mathbf{D}^{\alpha\alpha}(a) &= \Im\mathbf{D}^{\beta\beta}(a) = \mathbf{0} \; . \end{aligned} \quad (57)$$

Some comments on the above are in order. Eqs. (51) - (53) show us how to scale the real part of the $\alpha\beta$ and $\beta\alpha$ blocks of the density matrix, relative to their imaginary parts, or relative to the real part of the $\alpha\alpha$ and $\beta\beta$ blocks. However, those equations do not tell us, for example, how to scale the $\alpha\beta$ block relative to the $\beta\alpha$ block, as the magnetization is only defined through the sum or difference of their real or imaginary parts. In Eq. (57) we arbitrarily scale the $\alpha\beta$ and $\beta\alpha$ blocks equally with the factors of 1/2. Eqs. (51) - (53) also do not tell us how to scale the imaginary parts of the $\alpha\alpha$ and $\beta\beta$ blocks, as these are not used to build the magnetization and we therefore set them to zero. Nonetheless, we note that these blocks of the density matrix enter the definition of the orbital current-density.[61,62]

We finally note that each individual atomic density matrix $\mathbf{D}(a)$ is defined using a collinear magnetization, whose direction is determined by that of the vector $\underline{\mathbf{w}}(a)$. But since the total density matrix is obtained as a superposition of the $\mathbf{D}(a)$, the guess magnetization is in general non-collinear everywhere in space.

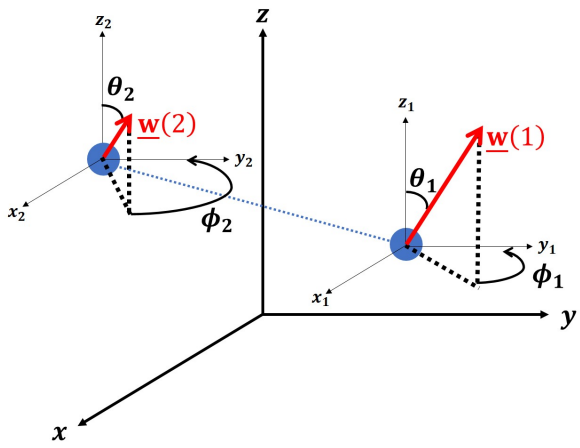

FIG. 1. Definition of the angles θ_a and ϕ_a in a generic bi-atomic molecule. A global Cartesian frame x, y, z is used to orient the atoms of the molecule, then local frames x_1, y_1, z_1 and x_2, y_2, z_2 are defined on each atomic center in order to orient the angles θ_1, ϕ_1 and θ_2, ϕ_2, which in turn manipulate the corresponding atomic density matrices. In this plot, the zx quadrant is in the plane of the page, so that the angles θ_a are those between the z axis and the zx projection of the vectors $\underline{\mathbf{w}}(a)$. The angles ϕ_a are those starting from the x axis and finishing at the xy projection of the corresponding $\underline{\mathbf{w}}(a)$.

III. COMPUTATIONAL DETAILS

We have implemented our two-component spin-orbit HF approach in a developmental version of the CRYSTAL17 code.[26] For the purposes of validating our implementation, as well as to discuss some of its performance and numerical stability aspects, we have chosen a test set of small molecular systems, and have performed similar calculations also with the latest public versions of the NWCHEM,[21] DIRAC[25] and TURBOMOLE[23] codes. The systems are the I_2, CH_3I, IH and TlBr molecules, in both a neutral state (closed-shell electronic configurations) and a positively charged state obtained by removing one electron from the molecules (open-shell electronic configurations): namely, I_2^+, CH_3I^+, IH^+ and $TlBr^+$. All linear molecules are oriented arbitrarily along the z axis (unless otherwise specified), with a bond length of 2.67 Å for I_2, 2.80 Å for TlBr and 3.00 bohr for IH, which are the experimental bond lengths. The exact geometry of the CH_3I molecule is provided in the supplemental material.[63]

For the C and H atoms, we use a modified version of the all-electron double-zeta basis sets of Dunning,[64] as available in the basis set library of the HONDO95 package.[65] We also note in passing that a similar SOC treatment with two-component HF theory has been implemented by one of us in our local version of the HONDO95 program for internal tests against the CRYSTAL implementation. For the heavy atoms (I, Tl, Br) we use the fully relativistic (scalar+spin-orbit) RECPs of Dolg and co-

workers. Specifically, the ECP46MDF and ECP28MDF are used for I and Br, respectively,[66] while for Tl, the ECP60MDF is used.[67] The valence basis sets we use are the triple-zeta basis set of Martin and Sundermann for I,[68] the double-zeta basis set of Dolg and co-workers for Tl[66] and that of Peterson for Br.[69]

For calculations with the TURBOMOLE code, the existing implementation requires use of the resolution of identity (RI) approximation for at least the evaluation of the Coulomb integrals.[22] Such a procedure requires expansion of the Coulomb operator in an auxiliary basis set. Where available, we use the def2-QZVPP-2c expansion set, or otherwise if not available, the dhf-QZVP-2c set.[70]

Calculations involving comparison among different codes were considered to have converged when the difference in energy between two successive cycles did not exceed 1×10^{-9} Ha, unless otherwise specified. Calculations performed with only our implementation to discuss convergence issues and different metastable electronic configurations had a higher convergence tolerance on the energy of 1×10^{-15} Ha. In all codes, we turn off screening algorithms for the evaluation of integrals.

TABLE I. Energies for the closed-shell electronic configurations. The E_0 is the energy obtained without the SOC operator in the Hamiltonian, while the E_{SOC} is the corresponding energy with the SOC operator included, as obtained with our implementation. The $\Delta E_X = E_{SOC} - E_0$ is the SOC contribution to the energy as obtained with the code X = CRY (CRYSTAL), NW (NWCHEM), TUR (TURBOMOLE) or DIR (DIRAC). The $\Delta\Delta E_X = \Delta E_X - \Delta E_{CRY}$ is the difference between the SOC energy contribution computed with the program X and that with our implementation. All quantities are reported in atomic units (Ha). The hyphen indicates that the TlBr calculation could not be performed with DIRAC in the same way as the other codes (see text for more details).

	I_2	CH_3I	IH	TlBr
E_0	-22.3521093204	-50.7878214941	-11.7546358329	-184.7377075782
E_{SOC}	-22.3593120591	-50.7907490722	-11.7574699229	-184.7696802376
ΔE_{CRY}	-7.2027386×10^{-3}	-2.9275781×10^{-3}	-2.8340901×10^{-3}	-3.19726594×10^{-2}
ΔE_{DIR}	-7.2027394×10^{-3}	-2.9275781×10^{-3}	-2.8340898×10^{-3}	-
ΔE_{NW}	-7.2027373×10^{-3}	-2.9275777×10^{-3}	-2.8351312×10^{-3}	-3.19726605×10^{-2}
ΔE_{TUR}	-7.1918968×10^{-3}	-2.8855949×10^{-3}	-2.8124657×10^{-3}	-3.19722265×10^{-2}
$\Delta\Delta E_{DIR}$	-7.5×10^{-10}	$+4.5\times10^{-11}$	$+2.5\times10^{-10}$	-
$\Delta\Delta E_{NW}$	$+1.3\times10^{-09}$	$+4.0\times10^{-10}$	-1.0×10^{-06}	-1.1×10^{-09}
$\Delta\Delta E_{TUR}$	$+1.1\times10^{-05}$	$+4.2\times10^{-05}$	$+2.2\times10^{-05}$	$+4.3\times10^{-07}$

IV. RESULTS AND DISCUSSION

We start our discussion on the performed calculations by first comparing results obtained using our implementation with those calculated using other available codes, with the purpose of validating our implementation and commenting on relative numerical accuracies and performance. Next we will discuss the obtained solutions on the individual molecules in more detail in terms of their energy and spatial distribution of the magnetization. We start by presenting results on the neutral closed-shell electronic configurations for the four considered molecules, followed by the positively charged open-shell ones.

Table I presents the total energies (in Ha) of the five molecules in their neutral closed-shell electronic configurations as computed with our implementation with, E_{SOC}, and without, E_0, spin-orbit coupling. The SOC contribution to the energy is given as $\Delta E = E_{SOC} - E_0$. This quantity is reported as computed with our implementation, ΔE_{CRY}, and as obtained with other codes, ΔE_X with X=NW for NWCHEM, X=TUR for TURBOMOLE, and X=DIR for DIRAC. The last rows contain the quantities $\Delta\Delta E_X = \Delta E_X - \Delta E_{CRY}$, which are the differences of the SOC contribution to the energy as computed with the other codes with respect to our implementation.

For the case of TlBr, it was not possible to use the DIRAC code in exactly the same computational conditions as in the other codes. This is due to the fact that the RECP-SOC implementation in DIRAC is only avail-

TABLE II. Energies for the open-shell electronic configurations. See caption of Table I for a definition of all quantities. Values are given in atomic units (Ha).

	CH_3I^+	IH^+	$TlBr^+$
E_0	−50.4740537084	−11.4070207076	−184.4323009231
E_{SOC}	−50.4893057289	−11.4190407956	−184.4673452196
ΔE_{CRY}	-1.52520205×10^{-2}	-1.20200879×10^{-2}	-3.50442965×10^{-2}
ΔE_{NW}	-1.52519711×10^{-2}	-1.20231322×10^{-2}	-3.50442958×10^{-2}
ΔE_{TUR}	-1.50500491×10^{-2}	-1.18585439×10^{-2}	-3.50410198×10^{-2}
$\Delta\Delta E_{NW}$	$+4.9\times10^{-08}$	-3.0×10^{-06}	$+6.7\times10^{-10}$
$\Delta\Delta E_{TUR}$	$+2.0\times10^{-04}$	$+1.6\times10^{-05}$	$+3.3\times10^{-06}$

able with a basis of Cartesian Gaussian-type functions that differ from spherical Gaussian-type functions (used in our implementation as well as in NWChem and Turbomole ones) starting from angular momentum $l = 2$ (i.e. starting from d-type functions). Given that TlBr has occupied d orbitals in the valence, it was not possible to perform the comparison with Dirac in this case. For all other molecular systems, no $l = 2$ or higher angular momentum functions were included in the valence basis sets, so that we were able to perform the comparison.

From Table I, we see that the SOC contribution to the total energy is of the order of 10^{-3} for the I_2, CH_3I and IH molecules and of 10^{-2} for TlBr. The SOC contribution to the total energy computed with our implementation is very close to that obtained with other implementations (this is embodied in the $\Delta\Delta E_X$ quantity in the table). The differences of our spin-orbit contribution with that from NWChem and Dirac are always very low, being on the order of 10^{-9}, 10^{-10}, or even 10^{-11} Ha (which are on the same order as the convergence criterion of the SCF), apart from the one case of the IH molecule with NWChem where it is instead on the order of 10^{-6} Ha. We get a slightly less impressive agreement with the results from Turbomole due to the fact that the Coulomb operator is evaluated using the RI approximation in that program, which results in a partial loss of accuracy. In general, our implementation best compares with Dirac (when possible), followed by NWChem and lastly Turbomole. Overall, the $\Delta\Delta E_X$ are always several orders of magnitude smaller than the SOC contribution to the energy, which confirms the correctness of our implementations for closed-shell systems.

We now discuss results obtained on the open-shell electronic configurations. Table II is analogous to Table I, but now for the cases where one electron is removed from the molecules such that they are now open-shell systems. We do not yet report the energies on the I_2^+ molecule in Table II as convergence of the SCF is particularly challenging in this case and we obtained different energies using different codes. More details on the calculations for the I_2^+ molecule are presented below. As a matter of fact, we were only able to find the ground state (lowest-energy) solution using our implementation with a tighter convergence criterion on the energy of 10^{-15} Ha (i.e. the tightest possible tolerance for a code with double-precision) instead of 10^{-9} Ha, as used in the other calculations.

Now, with the electron removed from the molecules, the spin-orbit contribution to the energy is around five times bigger for CH_3I, four times bigger for IH and around ten percent larger for TlBr. The $\Delta\Delta E_X$ quantities given in Table II are very small and overall comparable to those obtained on the closed-shell electronic configurations. Hence, the correctness of our implementation is also confirmed for open-shell systems. The agreement with NWChem is particularly satisfactory while the comparison with Turbomole also in this case suffers from its approximated RI treatment of the Coulomb operator. We note that we were unable to perform comparable calculations with the Dirac code on open-shell electronic configurations as, to the best of our knowledge, it is not possible to perform single-determinant Kramers-unrestricted calculations with the Dirac code at present.

We now comment on the computational efficiency of our implementation compared to those of the other codes with the help of Table III, which reports the number of cycles needed to converge the SCF to the same criterion on the energy of 1×10^{-9} Ha for the different systems here investigated. Both closed-shell and open-shell electronic configurations are considered in the table. A similar table is also included in the supplemental material[63] for the same calculations, but where the SCF was con-

TABLE III. Number of cycles to converge the SCF with a threshold on the energy of 1×10^{-9} Ha for both closed-shell and open-shell electronic configurations. The "n.c." label is used to mark those calculations that we were unable to converge. The asterisk marks a case (CH_3I^+ with NWChem with the DIIS convergence accelerator) where the SCF converges to a higher energy solution (3.38×10^{-3} Ha higher) than the ground state solution. Hyphens mark those calculations that can not be performed with the Dirac code, as discussed in the text.

	closed-shell				open-shell		
	I_2	CH_3I	IH	TlBr	CH_3I^+	IH^+	$TlBr^+$
Without DIIS							
Crystal	17	15	13	15	365	18	195
NWChem	29	25	22	22	679	399	417
Turbomole	48	40	39	58	1345	547	767
Dirac	22	n.c.	15	-	-	-	-
With DIIS							
NWChem	10	12	10	13	38*	37	23
Dirac	9	20	10	-	-	-	-

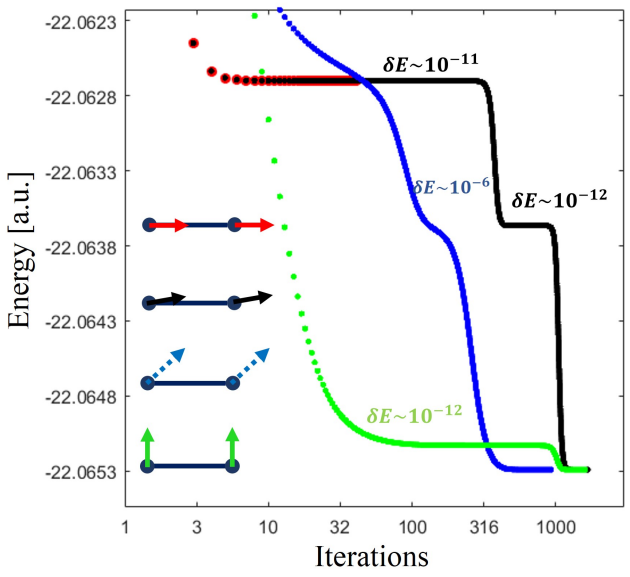

FIG. 2. Energy convergence profiles for the I_2^+ molecule. The evolution of the energy during the SCF iterations is shown, where both the energy and iterations are plotted on a logarithmic scale. The four curves of different colours correspond to the four initial guesses for the magnetization sketched on the left of the figure. The red guess is along the axis of the molecule (z axis). The black guess is one degree off of the axis of the molecule, towards the x direction. The blue guess is along the xyz diagonal (dashed lines are going out of the page). The green guess is oriented along x, that is to say perpendicular to the axis of the molecule. When the SCF passes through a plateau, the smallest difference in energy between two successive iterations is on the order of the δE of the corresponding colour. All calculations are eventually converged to 10^{-15} Ha.

verged instead to 1×10^{-7} Ha, where the same conclusions can be drawn. Results are first reported in the table without using the Direct Inversion in the Iterative Subspace (DIIS) convergence accelerator. For NWChem and Dirac, where DIIS is the default convergence accelerator option, we also report the number of cycles needed to converge when DIIS is activated. Again, default convergence options are used in all codes, with the exception of the possible deactivation of DIIS in NWChem and Dirac. For the case of the CH_3I molecule with Dirac and without DIIS, the "n.c." indicates that the calculation did not converge. For this discussion, it is noteworthy that the different programs use a different definition of the starting density matrix used to begin the SCF procedure. In the NWChem program, the starting guess density matrix is built from a superposition of non-relativistic atomic densities. In the Turbomole program, the guess density matrix is built from an extended Huckel calculation. Finally, in the Dirac program, the starting guess density matrix is obtained after the diagonalisation of a Fock matrix obtained from a superposition of atomic relativistic LDA potentials.

We first note that, when DIIS is not used, the open-shell calculations take a much greater amount of cycles to converge the SCF, than the closed-shell ones (around one order of magnitude more cycles, with the only notable exception of IH^+ with our implementation). The use of DIIS in Dirac and NWChem greatly reduces the amount of cycles needed to converge the SCF (by around a factor of 2 in closed-shell calculations, and by one order of magnitude in open-shell calculations). However, we stress that the use of DIIS may be undesirable in some cases as it might force convergence to a metastable state. For example, this is the case of the CH_3I^+ molecule (marked with an asterisk in the table) where the DIIS converges to a metastable state that is 3.38×10^{-3} Ha higher in energy than the ground state one. Only with deactivation of DIIS it was possible to converge to the ground state solution. Indeed, convergence problems of the DIIS algorithm for open-shell systems have been previously acknowledged several times in the litterature.[71–73]

When the DIIS is not used (what seems to be a safer strategy to get to the ground state solution), our implementation converges in much less SCF cycles than the other codes. That is, it converges in about two thirds to half the amount of cycles than the other codes for closed-shell calculations and in about half the amount of cycles for open-shell calculations. The exception, as already anticipated above, is the case of IH^+ where our implementation converges in an impressive 18 cycles when compared to the 399 cycles of NWChem or 547 cycles of Turbomole. We note that the relative number of cycles of the other codes follows the same order as for the $\Delta\Delta E_X$ in Tables I and II. That is, Dirac generally takes less cycles to converge than NWChem, followed by Turbomole. This points towards the conclusion that the amount of cycles needed to converge the SCF may very well be related to the overall numerical accuracy of the corresponding two-component HF implementation.

We now discuss in closer detail the obtained solutions for the individual charged molecules with open-shell electronic configurations. We start with the I_2^+ molecule. Given the self-consistent nature of our SOC treatment, it is interesting to discuss the evolution of the electronic configuration during the SCF process. A profile of the energy of the system along the SCF iterations is given in Figure 2, where both the energy and number of iterations are given on a logarithmic scale. Four different calculations are performed with different guesses for the initial orientation of the magnetization using the approach described in Section II C 5. The energies corresponding to the four guesses are plotted with different colours and the nature of the guess is sketched on the left of Figure 2. The red guess has the magnetization oriented along the axis of the molecule (z axis). The black guess has magnetization oriented one degree off of the axis of the molecule towards the x axis. The blue guess has the magnetization oriented along the xyz diagonal (i.e. equal amounts of m_x, m_y and m_z at the first iteration of the SCF). Finally,

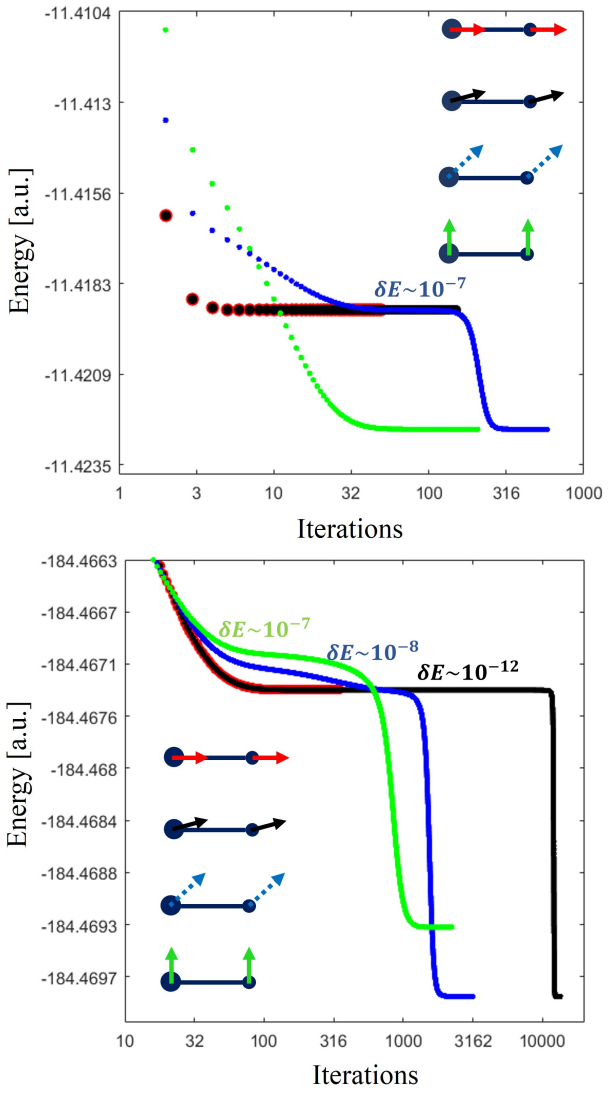

FIG. 3. Energy convergence profiles for the IH^+ (left panel) and $TlBr^+$ (right panel) molecules. The four curves of different colours correspond to the four initial guesses for the magnetization sketched in the insets of each panel. When the SCF passes through a plateau, the smallest difference in energy between two successive iterations is on the order of the δE of the corresponding colour. All calculations are eventually converged to 10^{-15} Ha.

the green guess has magnetization oriented along the x axis, that is to say perpendicular to the molecular axis.

All calculations are converged to 1×10^{-15} Ha, which is the highest possible threshold for a code working with double precision arithmetic, such as CRYSTAL. The green, blue and black guesses all lead to the same final ground state solution. This is not the case for the red guess, which leads to a metastable solution. Let us stress that in all the cases that eventually lead to the most stable ground state solution (green, blue, black), the SCF passes through plateaus (or regions of relatively flat energy profile) such that it appears as if the SCF procedure has converged. Nevertheless, if the convergence criteria on the energy is pushed far enough (as in our case), the SCF procedure eventually finds a lower energy solution. For example, in the case of the black curve, the SCF first reached a plateau after a few tens of iterations and for ∼300 iterations, where the lowest difference in energy between two successive cycles (denoted with δE in the figure) was of the order of 1×10^{-11} Ha. Then, the energy drops by $\sim 5 \times 10^{-4}$ Ha and the SCF again passes through a second plateau for another ∼600 iterations where the smallest δE is of the order of 1×10^{-12} Ha. Finally, the energy drops by another $\sim 15 \times 10^{-4}$ Ha and the ground state solution is found after 1672 iterations.

The fact that the SCF passes through plateaus with very small δE means that the ground state solution can only be found by using very tight convergence criteria on the energy, which means that the numerical accuracy and stability of the SOC-HF implementation becomes crucial for possibly reaching the ground state solution. In fact, in our efforts with DIRAC, NWCHEM, and TURBOMOLE, we were able at best to converge to the second plateau of the black curve, but never to the ground state solution. We note however, that as we are not authors of the DIRAC, NWCHEM, or TURBOMOLE codes, it is possible that certain options of which we are not aware might be available, which could improve the numerical accuracies of the calculations. The presence of the plateaus also highlights the importance of exploring different guesses for the initial magnetization distribution, as this sometimes permits the SCF to reach the ground state solution

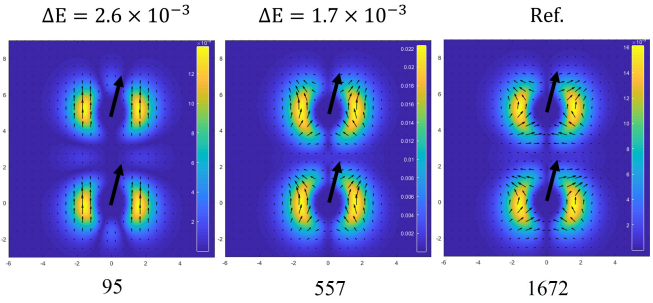

FIG. 4. Spatial distribution of the electronic magnetization $\mathbf{m}$ for the three electronic configurations corresponding to the three plateaus of the black curve in Figure 2 for the I_2^+ molecule. The first two panels correspond to metastable states while the last one to the ground state. The colour map represent the absolute value $|\mathbf{m}|$ of the magnetization in each point of the plane while the small black arrows represent the magnetization direction and relative magnitude. The two large black arrows represent the vectors $\underline{\mathbf{w}}(a)$ which define the orientation of the guess magnetization (one degree off of the axis of the molecule) on both centers. Differences in energies w.r.t. the lowest energy ground state solution are reported on top of the panels, while the amount of iterations needed to converge the SCF to the corresponding solutions is reported on the bottom of the figures. All quantities are reported in atomic units.

by bypassing some plateaus. For example, the blue curve only goes through one plateau, with a more manageable δE of 1×10^{-6} Ha, and reaches the lowest energy solution in ∼900 iterations (versus the ∼1700 of the black guess). In the red curve, on the other hand, the SCF gets stuck at the first plateau and the ground state solution is not obtained.

The importance of exploring different initial guesses for the orientation of the magnetization (in terms of effectiveness and efficiency in getting to the lowest energy solution) is documented even more clearly in the two panels of Figure 3, which is analogous to Figure 2, but now refers to the IH^+ and $TlBr^+$ molecules. Indeed, for both molecules, only two of the four explored guesses lead to the lowest energy solution: green and blue for IH^+ and blue and black for $TlBr^+$. As already observed for the I_2^+ linear molecule discussed above, also here the red guess with the magnetization aligned with the axis of the molecule produces a metastable electronic configuration. For IH^+, also the black guess (one degree tilted off the molecular axis) leads to the same metastable solution. For $TlBr^+$, the black guess also virtually converges to the same metastable state as the red one, being able to jump to the lowest energy solution only after some 10000 SCF iterations. For $TlBr^+$, the guess perpendicular to the molecule (green curve) leads to another solution intermediate in energy that is $\sim4\times10^{-4}$ Ha higher than the ground state solution. Let us stress that, in Table II, where we compared our description of IH^+ and $TlBr^+$ with that obtained from NWChem and Turbomole, the metastable electronic configuration obtained with the red guess was considered as we were unable to get the lowest energy solution with the other codes.

In order to further comment on the relevance of the initial guess in this kind of simulations, we note that in the case of the IH^+ a green guess with the magnetization perpendicular to the axis of the molecule leads to the lowest energy ground state electronic configuration in just some 50 iterations without passing through intermediate metastable states.

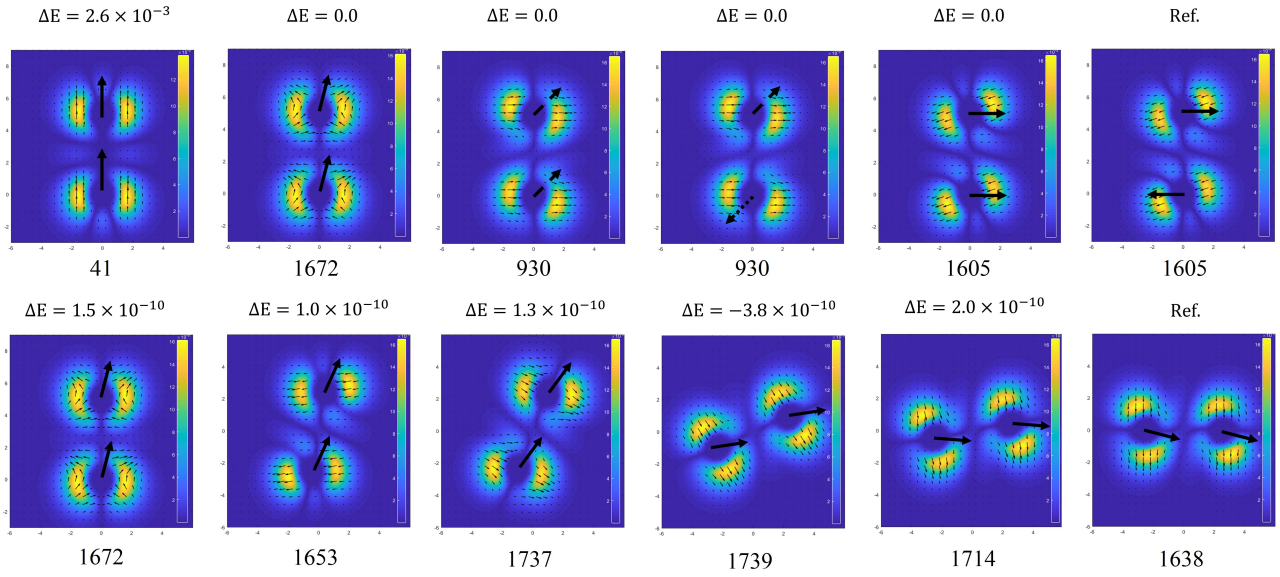

FIG. 5. Spatial distribution of the electronic magnetization **m** of the lowest energy solution of the I_2^+ molecule (top panels) as a function of different initial starting guesses, and (bottom panels) as the molecule is rotated from the z axis to the x axis with the same relative guess. The orientation of the initial guess for the magnetization on the two atomic centers is represented by the big black arrows. Differences in energies w.r.t. the right-most panel are reported on top of the panels, while the amount of iterations needed to converge the SCF to the corresponding solutions is reported on the bottom of the figures. All quantities are reported in atomic units.

So far we have discussed the energy of the different solutions found at the various plateaus of Figures 2 and 3 for the I_2^+, IH^+ and $TlBr^+$ molecules. Let us now have a closer look at their electronic structure, in particular in terms of electronic magnetization. In Figure 4, we present 2D maps of the non-collinear magnetization **m**, as introduced in Eq. (50), for the three electronic configurations corresponding to the three plateaus of the

black curve in Figure 2 for the I_2^+ molecule. The colour map represent the absolute value $|\mathbf{m}|$ of the magnetization in each point of the plane while the small black arrows represent the magnetization direction and relative magnitude. The two large black arrows at the two atomic centers represent the vectors $\underline{\mathbf{w}}(a)$ in Eq. (56), which define the orientation of the guess magnetization (one degree off of the axis of the molecule in this case) on both centers.

Figure 4 helps to show that rather different spin textures can be obtained by pushing the SCF to higher tolerances. The first metastable solution (left panel) corresponds to the first plateau of the black curve in Figure 2, is 2.6×10^{-3} Ha higher in energy than the ground state, and is characterized by a magnetization that is almost aligned parallel to the axis of the molecule everywhere. The second metastable solution (middle panel) corresponds to the second plateau of the black curve in Figure 2, is 1.7×10^{-3} Ha higher in energy than the ground state, and is characterized by a distribution of magnetization no longer aligned to the axis of the molecule, which resembles more closely the one of the ground state (right panel). The solutions obtained for the I_2^+ molecule along the other curves of Figure 2 are included in the supplemental material.[63] We also provide similar figures for the ground state and metastable solutions of the IH^+ and $TlBr^+$ molecules in the supplementary information.

Now, we want to discuss two other aspects: i) the existence of different degenerate solutions characterized by the same energy but different spin texture (i.e. spatial distribution of the magnetization), and ii) the rotational invariance of our SOC-HF implementation. In Figure 5, we report the spatial distribution of the electronic magnetization $\mathbf{m}$ of the lowest energy solution of the I_2^+ molecule as a function of different initial starting guesses (top panels), and as the molecule is rotated from the z axis to the x axis with the same relative guess (bottom panels). The orientation of the initial guess for the magnetization on the two atomic centers is represented by the big black arrows.

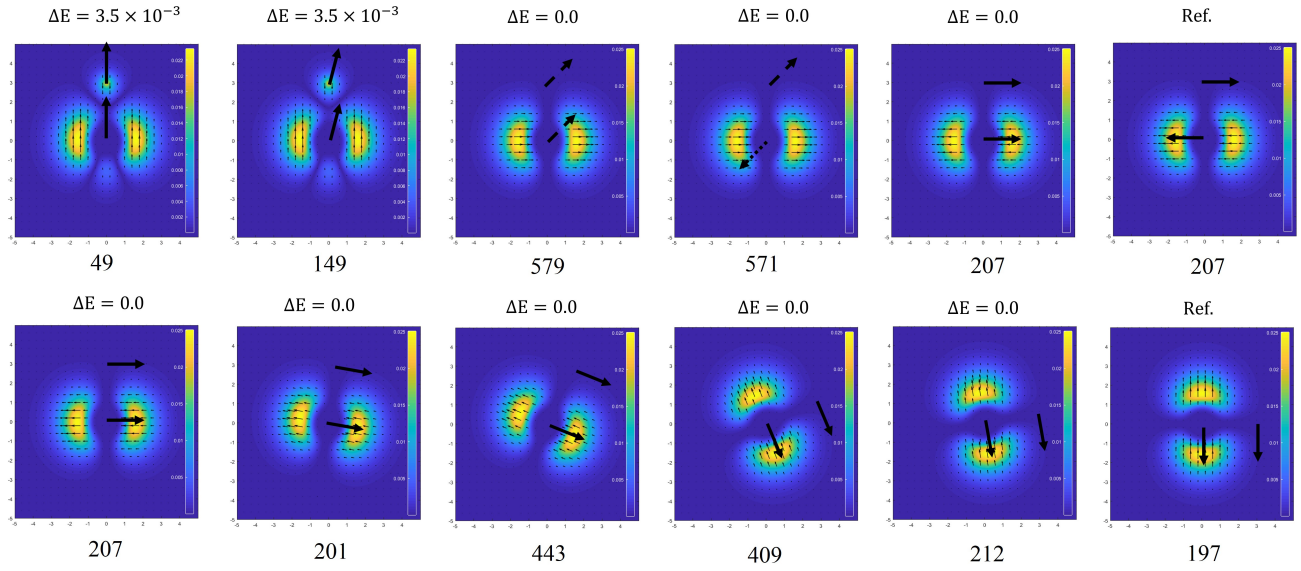

FIG. 6. Same as Figure 5 for the IH^+ molecule.

Let us first discuss the different solutions obtained by starting from different guesses (six top panels). The first guess is oriented along the axis of the molecule, the second is oriented one degree off of the axis of the molecule, the third is along the xyz diagonal (with dashed line pointing outside of the page), the fourth is along the xyz diagonal along one center and the $-x-y-z$ diagonal along the other center (with dotted line pointing inside the page), the fifth is perpendicular to the molecular axis (along the x axis), and the sixth is again perpendicular to the molecular axis, but on one center along the x direction and on the other center along the $-x$ direction.

Five out of six initial guesses (panels 2 to 6 in the figure) eventually lead to the lowest energy ground state. The only guess that leads to a metastable solution (3.5×10^{-3} Ha higher in energy) is the one perfectly aligned with the axis of the molecule (panel 1). From the analysis of the five energy-degenerate solutions, we can

identify three distinct spin textures: that of the second panel (where the magnetization changes its orientation around the atoms), that of panels 3 and 4 (with a magnetization along x, almost perpendicular to the axis of the molecule), and that of panels 5 and 6 (with a magnetization aligned along a common direction everywhere and slightly tilted with respect to the x axis).

The six panels on the bottom of Figure 5 show the lowest energy solution as the axis of the molecule rotates from z to x where we always use the same relative guess (one degree off of the molecular axis). Here, we want to check the rotational invariance of our implementation, which should be ensured by the formalism presented in Section II C. Rotational invariance is a property that becomes crucial in the extension of the treatment of SOC within the DFT, as we are going to discuss into detail in Part II of this paper. From Figure 5, we see that the rotational invariance is achieved within a numerical accuracy of the order of 10^{-10} Ha (the maximum energy difference between different orientations being 3.8×10^{-10}), which overall confirms the high accuracy of the implementation. We note that, as the molecule is rotated, the obtained solution hops among the three degenerate spin textures discussed above.

A similar analysis to the one just performed on the I_2^+ molecule is reported in Figure 6 for the IH^+ molecule. On the top panels, four of the six different guesses converge to the same lowest energy solution characterized by magnetization always perpendicular to the axis of the molecule and only around the I atom. The first two panels show the metastable electronic configuration (3.5×10^{-3} Ha higher in energy), corresponding to the red and black plateaus in Figure 3, with magnetization parallel (and antiparallel) to the axis of the molecule with a non null magnetization on the H atom. On the bottom six panels, rotational invariance is perfectly achieved in this case down to double precision, as the energy differences are exactly null (i.e. $< 10^{-15}$ Ha). A similar plot to Figures 5 and 6 is given in the supplemental material[63] for the $TlBr^+$ molecule, where similar considerations can be made.

V. CONCLUSIONS AND PERSPECTIVES

We have revised the formalism of the Kramers-unrestricted generalisation of the Hartree-Fock (HF) theory for the self-consistent treatment of spin-orbit coupling in electronic structure calculations, where the wavefunction is expanded in terms of complex two-component spinors. Some constraints of standard one-component implementations of spin-unrestricted HF need to be relaxed so as to deal with the new $\alpha\beta$ and $\beta\alpha$ blocks in the description of the electronic configurations, especially for open-shell systems.

We have illustrated a molecular implementation in the CRYSTAL program, of such methodology where spin-orbit and scalar-relativistic operators are defined through relativistic effective-core potentials. The correctness of the implementation, as well as its accuracy and efficiency, is discussed by comparison to three other existing similar implementations through tests on small molecules.

A new approach is presented for generalising a non- or scalar-relativistic atomic guess density matrix to impose a desired non-collinear magnetization as a starting point of the SCF procedure. The importance of using such an approach is highlighted on some test examples on small molecular systems, where it is shown that in all of the tested cases, the ground state solution can be found only through such modification of the guess. Some confidence in the fact that the final solution represents the global minimum of the total energy can be gained if several choices of the starting guess lead to the same energy.

In Part II of the paper, we will discuss the self-consistent treatment of spin-orbit coupling effects within collinear and non-collinear DFT (in its local density, generalised-gradient and hybrid formulations). In particular, we will address the accuracy, numerical robustness, and computational efficiency of the different flavors of non-collinear DFT reported in the literature and we will present a new formulation, which ensures higher numerical stability and efficiency. In the context of DFT calculations, we will stress the importance of including a fraction of exact Fock exchange (whose treatment in SOC calculations has been discussed in this paper), through hybrid functionals, to get a physically sound description of local magnetic torque and orbital current-density.

The extension of the presented methodology to the description of extended periodic systems represents a near-future development and will be presented in forthcoming publications.

SUPPLEMENTARY MATERIAL

See supplementary material for the geometry of the CH_3I molecule, the number of cycles needed to converge the SCF to $1 \cdot 10^{-7}$ a.u. in energy, spatial distributions of the magnetization for meta-stable solutions for the I_2^+, IH^+ and $TlBr^+$ molecules, and final distributions of the magnetization for different guesses for the $TlBr^+$ molecule as well as for different orientations of the molecular axis.

ACKNOWLEDGEMENTS

We are grateful to Russell Pitzer for letting us use his routines for calculation of SOC-RECP integrals and to Valerie Vallet for her contribution in modifying these routines to include them in her SO-CI program (called EPCISO, from Ref. 5), which were the same SOC-RECP integral routines that we implemented in HONDO and CRYSTAL. We thank Michael Dolg for taking the time to come to Torino for useful discussions on the use of his set of RECPs. J.K.D. is grateful to the National Science

and Engineering Research Council of the Government of Canada for a Vanier scholarship.

Appendix: Working Expressions for the Evaluation of the Energy

Here we show how the four terms in Eq. (46) can be developped into working expressions in terms of the $\sigma\sigma'$ spin-blocks. This is useful to allow for the exploitation of the symmetry properties for the various integral types. From the Hermiticity of $\mathbf{K}$ and $\mathbf{D}$, the exchange term yields:

$$\begin{aligned}\Re\left[\mathrm{Tr}\left(\mathbf{K}\mathbf{D}^\dagger\right)\right] &= \mathrm{Tr}(\Re\mathbf{K}^{\alpha\alpha}\Re\mathbf{D}^{\alpha\alpha\,\dagger}) - \mathrm{Tr}(\Im\mathbf{K}^{\alpha\alpha}\Im\mathbf{D}^{\alpha\alpha\,\dagger}) \\ &+ \mathrm{Tr}(\Re\mathbf{K}^{\beta\beta}\Re\mathbf{D}^{\beta\beta\,\dagger}) - \mathrm{Tr}(\Im\mathbf{K}^{\beta\beta}\Im\mathbf{D}^{\beta\beta\,\dagger}) \\ &+ 2\mathrm{Tr}(\Re\mathbf{K}^{\alpha\beta}\Re\mathbf{D}^{\alpha\beta\,\dagger}) - 2\mathrm{Tr}(\Im\mathbf{K}^{\alpha\beta}\Im\mathbf{D}^{\alpha\beta\,\dagger}) \quad \text{(A.1)}\end{aligned}$$

From the Hermiticity of $\mathbf{h}_0$, $\mathbf{C}$ and $\mathbf{D}$, the SR and Coulomb terms yield:

$$\Re\left[\mathrm{Tr}(\mathbf{A}\mathbf{D}^\dagger)\right] = \mathrm{Tr}(\Re\mathbf{A}^{\alpha\alpha}\Re\mathbf{D}^{\alpha\alpha\,\dagger}) + \mathrm{Tr}(\Re\mathbf{A}^{\beta\beta}\Re\mathbf{D}^{\beta\beta\,\dagger}) \quad \text{(A.2)}$$

where $\mathbf{A} = \mathbf{C}$ or $\mathbf{h}_0$. Finally, the symmetry properties of $\mathbf{h}_{\mathrm{SO}}$ from Eqs. (33) and (34), as well as the Hermiticity of $\mathbf{D}$, yield:

$$\begin{aligned}\Re\left[\mathrm{Tr}(\mathbf{h}_{\mathrm{SO}}\mathbf{D}^\dagger)\right] &= -\mathrm{Tr}\Big(\Im\mathbf{h}_{\mathrm{SO}}^{\alpha\alpha}\big[\Im\mathbf{D}^{\alpha\alpha\,\dagger} - \Im\mathbf{D}^{\beta\beta\,\dagger}\big]\Big) \\ &+ 2\mathrm{Tr}(\Re\mathbf{h}_{\mathrm{SO}}^{\alpha\beta}\Re\mathbf{D}^{\alpha\beta\,\dagger}) - 2\mathrm{Tr}(\Im\mathbf{h}_{\mathrm{SO}}^{\alpha\beta}\Im\mathbf{D}^{\alpha\beta\,\dagger}) \quad \text{(A.3)}\end{aligned}$$

or equivalently:

$$\begin{aligned}\Re\left[\mathrm{Tr}(\mathbf{h}_{\mathrm{SO}}\mathbf{D}^\dagger)\right] &= -\mathrm{Tr}\Big(\Im\mathbf{h}_{\mathrm{SO}}^{\alpha\alpha}\big[\Im\mathbf{D}^{\alpha\alpha\,\dagger} - \Im\mathbf{D}^{\beta\beta\,\dagger}\big]\Big) \\ &+ 2\tilde{\mathrm{Tr}}(\Re\mathbf{h}_{\mathrm{SO}}^{\alpha\beta}\big[\Re\mathbf{D}^{\alpha\beta\,\dagger} + \Re\mathbf{D}^{\beta\alpha\,\dagger}\big]) \\ &- 2\tilde{\mathrm{Tr}}(\Im\mathbf{h}_{\mathrm{SO}}^{\alpha\beta}\big[\Im\mathbf{D}^{\alpha\beta\,\dagger} - \Im\mathbf{D}^{\beta\alpha\,\dagger}\big]) \quad \text{(A.4)}\end{aligned}$$

where the $\tilde{\mathrm{Tr}}$, is the half trace, and means that the trace is taken over the first half of the diagonal elements.

[1] K. G. Dyall and K. Faegri, *Introduction to relativistic quantum chemistry* (Oxford University Press on Demand, 2007).
[2] P. Pyykkö, Ann. Rev. Phys. Chem. **63**, 45 (2012).
[3] T. Saue, Chem. Phys. Chem. **12**, 3077 (2011).
[4] P. W. Atkins and R. S. Friedman, *Molecular quantum mechanics* (Oxford university press, 2011).
[5] V. Vallet, L. Maron, C. Teichteil, and J.-P. Flament, J. Chem. Phys. **113**, 1391 (2000).
[6] S. Yabushita, Z. Zhang, and R. M. Pitzer, J. Phys. Chem. A **103**, 5791 (1999).
[7] P. Pyykko and J. P. Desclaux, Acc. Chem. Res. **12**, 276 (1979).
[8] A. Wolf, M. Reiher, and B. A. Hess, J. Chem. Phys. **117**, 9215 (2002).
[9] L. L. Foldy and S. A. Wouthuysen, Phys. Rev. **78**, 29 (1950).
[10] E. v. Lenthe, E.-J. Baerends, and J. G. Snijders, J. Chem. Phys. **99**, 4597 (1993).
[11] J. G. Snijders and A. J. Sadlej, Chem. Phys. Lett. **252**, 51 (1996).
[12] K. G. Dyall and E. van Lenthe, J. Chem. Phys. **111**, 1366 (1999).
[13] C. Chang, M. Pelissier, and P. Durand, Phys. Sc. **34**, 394 (1986).
[14] W. Liu, Mol. Phys. **108**, 1679 (2010).
[15] M. Dolg, in *Theor. Comput. Chem.* (Elsevier, 2002), vol. 11, pp. 793–862.
[16] R. M. Pitzer and N. W. Winter, Int. J. Q. Chem. **40**, 773 (1991).
[17] M. Dolg and X. Cao, Chem. Rev. **112**, 403 (2011).
[18] P. Schwerdtfeger, ChemPhysChem **12**, 3143 (2011).
[19] A. Weigand, X. Cao, V. Vallet, J.-P. Flament, and M. Dolg, J. Phys. Chem. A **113**, 11509 (2009).
[20] Z. Zhang, Theor. Chem. Acc. **133**, 1588 (2014).
[21] M. Valiev, E. J. Bylaska, N. Govind, K. Kowalski, T. P. Straatsma, H. J. Van Dam, D. Wang, J. Nieplocha, E. Apra, T. L. Windus, et al., Comput. Phys. Comm. **181**, 1477 (2010).
[22] M. K. Armbruster, F. Weigend, C. van Wüllen, and W. Klopper, Phys. Chem. Chem. Phys. **10**, 1748 (2008).
[23] *TURBOMOLE V7.3 2018, a development of University of Karlsruhe and Forschungszentrum Karlsruhe GmbH, 1989-2007, TURBOMOLE GmbH, since 2007; available from* `http://www.turbomole.com`.
[24] Y.-C. Park, I. S. Lim, and Y.-S. Lee, Bull. Kor. Chem. Soc. **33**, 803 (2012).
[25] DIRAC, a relativistic ab initio electronic structure program, Release DIRAC17 (2017), written by L. Visscher, H. J. Aa. Jensen, R. Bast, T. Saue, and others (see `http://www.diracprogram.org`).
[26] R. Dovesi, A. Erba, R. Orlando, C. M. Zicovich-Wilson, B. Civalleri, L. Maschio, M. Rérat, S. Casassa, J. Baima, S. Salustro, et al., WIRES Comput. Mol. Sci. p. e1360 (2018).
[27] G. Kresse and J. Furthmüller, Phys. Rev. B **54**, 11169 (1996).
[28] P. Blaha, An augmented plane wave+ local orbitals program for calculating crystal properties (2001).
[29] D. Koelling and B. Harmon, J. Phys. C **10**, 3107 (1977).
[30] P. Kurz, F. Förster, L. Nordström, G. Bihlmayer, and S. Blügel, Phys. Rev. B **69**, 024415 (2004).
[31] P. Giannozzi, S. Baroni, N. Bonini, M. Calandra, R. Car, C. Cavazzoni, D. Ceresoli, G. L. Chiarotti, M. Cococcioni, I. Dabo, et al., J. Phys. Condens. Matt. **21**, 395502 (2009).
[32] P. Giannozzi, O. Andreussi, T. Brumme, O. Bunau, M. B. Nardelli, M. Calandra, R. Car, C. Cavazzoni, D. Ceresoli, M. Cococcioni, et al., J. Phys. Condens. Matt. **29**, 465901 (2017).
[33] A. Dal Corso and A. M. Conte, Phys. Rev. B **71**, 115106 (2005).
[34] G. Te Velde and E. Baerends, Phys. Rev. B **44**, 7888 (1991).
[35] R. Sakuma, C. Friedrich, T. Miyake, S. Blügel, and F. Aryasetiawan, Phys. Rev. B **84**, 085144 (2011).
[36] P. Scherpelz, M. Govoni, I. Hamada, and G. Galli, J. Chem. Theor. Comput. **12**, 3523 (2016).
[37] M. Kadek, M. Repisky, and K. Ruud, Phys. Rev. B **99**, 205103 (2019).
[38] J. Desmarais, J. Flament, and A. Erba, J. Chem. Phys. (2019), under review.
[39] M. Blume and R. Watson, Proc. Roy. Soc. Lond. **270**, 127 (1962).
[40] M. Blume, Phys. Rev. **133**, A1366 (1964).
[41] S. Murakami, Phys. Rev. Lett. **97**, 236805 (2006).
[42] R. Wu and A. J. Freeman, J. Magn. Magn. Mater. **200**, 498 (1999).
[43] Q. Zeng, X. Chu, M. Yang, and D.-Y. Wu, Chem. Phys. **395**, 82 (2012).
[44] M. Tsujikawa, A. Hosokawa, and T. Oda, Phys. Rev. B **77**, 054413 (2008).
[45] G. E. Pacchioni, L. Gragnaniello, F. Donati, M. Pivetta, G. Autes, O. V. Yazyev, S. Rusponi, and H. Brune, Phys. Rev. B **91**, 235426 (2015).
[46] K. E. El-Kelany, C. Ravoux, J. K. Desmarais, P. Cortona, Y. Pan, J. Tse, and A. Erba, Phys. Rev. B **97**, 245118 (2018).
[47] Y. S. Lee, W. C. Ermler, and K. S. Pitzer, in *Molecular Structure And Statistical Thermodynamics: Selected Papers of Kenneth S Pitzer* (World Scientific, 1993), pp. 112–127.
[48] H. Stoll, B. Metz, and M. Dolg, J. Comput. Chem. **23**, 767 (2002).
[49] L. Maron and C. Teichteil, Chem. Phys. **237**, 105 (1998).
[50] W. C. Ermler, Y. S. Lee, P. A. Christiansen, and K. S. Pitzer, in *Molecular Structure And Statistical Thermodynamics: Selected*

Papers of Kenneth S Pitzer (World Scientific, 1993), pp. 176–180.
[51]L. E. McMurchie and E. R. Davidson, J. Comput. Phys. **44**, 289 (1981).
[52]X. Cao and M. Dolg, Coor. Chem. Rev. **250**, 900 (2006).
[53]R. M. Pitzer and N. W. Winter, J. Phys. Chem. **92**, 3061 (1988).
[54]J. K. Desmarais, A. Erba, and R. Dovesi, Theor. Chem. Acc. **137**, 28 (2018).
[55]J. Valatin, Phys. Rev. **122**, 1012 (1961).
[56]M. Reiher, Far. disc. **135**, 97 (2007).
[57]C. Van Wüllen, J. Comput. Chem. **23**, 779 (2002).
[58]K. Capelle, G. Vignale, and B. Györffy, Phys. Rev. Lett. **87**, 206403 (2001).
[59]P. J. Cherry, S. Komorovsky, V. G. Malkin, and O. L. Malkina, Mol. Phys. **115**, 75 (2017).
[60]E. Clementi, *Modern techniques in computational chemistry: MOTECC-91*, vol. 91 (Springer Science & Business Media, 1991).
[61]C. van Wüllen, in *Theor. Comput. Chem.* (Elsevier, 2004), vol. 14, pp. 598–655.
[62]J. Desmarais, J. Flament, and A. Erba, J. Phys. Chem. Lett. **10**, 3580 (2019).
[63]See Supplemental Material at URL for the geometry of the CH_3I molecule, for a table on the computational efficiency of our implementation compared to existing ones, for plots of the spatial distribution of the magnetization of meta-stable states of the studied molecules, a plot showing the rotational invariance for the $TlBr^+$ molecule.
[64]T. H. Dunning Jr, J. Chem. Phys. **53**, 2823 (1970).
[65]M. Dupuis, A. Farazdel, S. Kama, and S. Maluendes, IBM Corporation, Center for Scientific & Engineering Computations, Kingston, New York **115**, 1153 (1991).
[66]H. Stoll, B. Metz, and M. Dolg, J. Comput. Chem. **23**, 767 (2002).
[67]B. Metz, M. Schweizer, H. Stoll, M. Dolg, and W. Liu, Theor. Chem. Acc. **104**, 22 (2000).
[68]J. M. Martin and A. Sundermann, J. Chem. Phys. **114**, 3408 (2001).
[69]K. A. Peterson, J. Chem. Phys. **119**, 11099 (2003).
[70]F. Weigend, J. Comput. Chem. **29**, 167 (2008).
[71]P. Pulay and R. F. Liu, J. Phys. Chem. **94**, 5548 (1990).
[72]Q. Sun, arXiv preprint arXiv:1610.08423 (2016).
[73]F. Neese, Chem. Phys. Lett. **325**, 93 (2000).